UNIVERSITY OF CALIFORNIA
RIVERSIDE

Harnessing Triplet Excitons in Hybrid Nanocrystal-Molecule Systems to Power Photon Upconversion in Solution and Solid State

A Dissertation submitted in partial satisfaction
of the requirements for the degree of

Doctor of Philosophy

in

Chemistry

by

Emily Meredith Moses Rigsby

December 2020

Dissertation Committee:
Dr. Ming Lee Tang, Chairperson
Dr. Leonard J. Mueller
Dr. Chia-en Chang

The Dissertation of Emily Meredith Moses Rigsby is approved:

_____

_____

_____

Committee Chairperson

University of California, Riverside

Acknowledgements

First, I would like to acknowledge my advisor, Dr. Ming Lee Tang, who reached out when she noticed I was not meeting my full potential as a graduate student and pushed me to do more in my doctoral research. Through her mentorship, I was able to grow and experience some of the most academically rewarding events of my career, both domestic and international.

I would also like to thank my committee and collaborators for their excellent mentorship through my research: Dr. Chris Bardeen, Dr. Lenard Muller, Dr. Cha en Chang, Dr. Jack Eichler, and Dr. Nathaniel Gabor for their efforts here at UCR and Dr. Sean Roberts, Dr. Nobuhiro Yanai, Dr. Nobuo Kimizuka, and Dr. Dima Fishman for their fruitful collaborations and guidance.

I would like to thank Dr. Bruce Schilling for believing in my abilities, fostering my love of chemistry, and guiding me into graduate school. Without his calm response every time I fused my glassware together, mentorship through managing the teaching labs, and ample supplies of pumpkin bread, I would not be where I am today.

I would like to thank the communities I have become a part of here in Southern California. Thank you to my laboratory community: to Zhiyuan Huang, Xin Li, Melika Mahboub, and Pan Xia, the senior graduate students who mentored me, and to Carter, Paulina Jaimes, Tingting Huang, Tsumugi Miyashita, Kefu Wang, Zhongxiang Wang, Michael Olsen, Kevin Lee, and Tiffany Tran, the junior graduate students and undergraduates who helped me and brightened life in lab. Thank you all for enriching my

graduate school experience. And thank you also to my Rooted community and extended family who mentored and loved me outside of the lab.

Finally, I would like to thank my incredible family for their unwavering love and support. To my parents, I owe everything, and I know I would not have made it through without them. And to my husband Ryan, thank you for being my rock and my light. Thank you for believing in me, even when I did not. I feel so grateful every day to have you in my life.

ABSTRACT OF THE DISSERTATION

Harnessing Triplet Excitons in Hybrid Nanocrystal-Molecule Systems to Power Photon Upconversion in Solution and Solid State

by

Emily Meredith Moses Rigsby

Doctor of Philosophy, Graduate Program in Chemistry
University of California, Riverside, December 2020
Dr. Ming Lee Tang, Chairperson

Photon upconversion is the process where two low energy photons combine to form one higher energy photon. This two-photon process has many diverse applications in solar energy conversion, catalysis, and bioimaging. Molecular triplet-triplet annihilation (TTA) based upconversion benefits from using inorganic nanocrystal (NC) sensitizers because this hybrid system combines the stability and absorption properties of inorganic semiconductors with the high efficiencies of TTA in conjugated organic materials.

In TTA based photon upconversion, controlling triplet energy transfer (TET) through the system is key to unlocking higher efficiencies. This dissertation focuses on better understanding this TET process and how this knowledge can be used to optimize inorganic-organic hybrid upconversion systems as we transition to solid state thin film applications. Primary amines are used to better understand how the large surface area of nanocrystals impacts TET. The introduction of primary amines increases the upconversion quantum yield approximately 5-fold with further additions of amine not improving photon

upconversion, as CdSe NC photoluminescence (PL) increases at the expense of triplet energy transfer. Transient absorption measurements show that the amines enhance NC PL by decreasing the nonradiative decay rate, increasing the rate of triplet energy transfer, and enable the broad trap state in these CdSe NCs to participate in triplet photosensitization.

Further understanding of TET is found by size dependence studies of the CdSe nanocrystal sensitizer. As CdSe NC size increases the photon upconversion quantum yield (QY) decreases due to the decrease in the driving force for TET from CdSe to the surface bound transmitter ligand, as expected for the Marcus description of energy transfer from the transmitter to the NC. Long microsecond transmitter lifetimes are critical to high photon upconversion QYs.

Ultimately, these enhancements in efficiencies pave the way for a transition to high efficiency thin film upconverting materials, which already show promise by exhibiting high efficiencies, increased stability, and reduction in reliance on organic solvents over solution-based systems. The future of useful upconverting materials relies on taking this understanding of energy transfer in nanocrystals and applying it to biocompatible upconverting thin films.

Table of Contents

List of Figures

List of Tables

Chapter 1 Introduction

1.1 Introduction to photon upconversion

Triplet-triplet annihilation (TTA) based upconversion is a process where a sensitizer absorbs a long-wavelength photon, transitions the energy to the triplet state, and then to separate emitter molecules. Once the emitter molecules have the triplet energy, two neighboring triplet excited states combine via spin allowed TTA into one molecule with a higher energy excited state (S_1) and one in the ground state. The molecule with the newly populated singlet state can then emit a higher energy photon. By developing and implementing a TTA upconversion system, two low energy photons can be utilized to create one high energy photon. TTA based upconversion systems can be used wherever higher energy photons are needed. In medicine, high energy photons can be used to treat cancer, kill bacteria, and power optogenetics or light activation of proteins.[1-3] In each of these cases, low energy red light can be used to produce the high energy light precisely where it is needed, limiting damaging exposure.

1.2 Why use a Hybrid Molecule-Nanocrystal Upconversion System?

The highest internal upconversion efficiencies have been observed in lanthanides ions; however, these materials require high power densities, are only useful in narrow spectral regions, and the forbidden optical transitions mandates the use of optically thick films. Molecular systems based on the TTA properties of conjugated organic molecules produce lower absolute quantum yield efficiencies but have more promise under solar flux and are adaptable into thin film applications. Even with these advantages, purely organic

systems are especially poor candidates for solar and biological applications because no organic system currently absorbs in the IR region of interest while having the long-term stability of their inorganic counterparts. Nanocrystal (NC) organic hybrid systems combine the stability and absorption properties of inorganic semiconductors with the flexibility of TTA in conjugated organic materials.[4-5] Using quantum dots as absorbers greatly increases the tunability, as well as stability, of absorption, providing a best-case scenario for designing ideal upconversion systems for diverse applications. While these systems are currently 20% efficient,[6] high efficiencies and the removal of organic solvents are needed for widespread applications.

1.3 Diving deeper to understand triplet energy transfer

In the past, aliphatic amines have been observed to both enhance and quench the photoluminescence quantum yield (PLQY) of CdSe nanocrystals,[7-8] and studying how these amines affect triplet energy transfer in photon upconversion provides a clearer picture of how energy moves throughout the system. When the CdSe NCs are functionalized with 2-anthracene carboxylic acid ligand, the photon upconversion quantum yield increased by up to 4.4 times in the presence of propylamine. Transient absorption spectroscopy allows for time-resolved probing deeper into the energy processes, showing that propylamine enhances triplet energy transfer in two ways: first, by decreasing the contribution of the non-radiative decay processes in the CdSe NC, and second, by increasing the rate of triplet energy transfer.[9] This structural information about the amine-nanocrystal interface is key to better understanding the role these surface states play in energy transfer and offers practical routes towards optimizing hybrid organic-inorganic upconversion system.

1.4 Solid state upconverting thin film materials

To step closer towards functional and durable upconversion materials for solar and medical applications, much work is being done currently to make efficient upconverting thin films, which transition these materials from solution to solid state. In this process, many drawbacks to practical applications, such as toxic organic solvents and long-term instability, are being addressed.

1.5 Physically mixed glassy polymer photon upconverting thin films

The first TTA based upconverting thin films were made by Castellano et al. in 2007.[10] These films built upon the work of Parker and Hatchard's triplet sensitizing organic chromophores[11] by using a metal-organic chromophore embedded with DPA in an ethyleneoxide/epichlorohydrin copolymer P(EO/ EP). These polymer films were cast onto glass microscopy slides, annealed at 90 °C for 5 min, and built up to three layers for a final thickness of 100 μm. After allowing to dry in the dark for a least 1 week, portions of the upconverting films displayed DPA phase separation due to high emitter concentrations. While these films showed early success, the researchers did not highlight their low quantum efficiencies for the films, instead pointing to the low (6 to 27 mW/cm^2) power densities required. They found that, as in solution, the emission signal is proportional to the DPA triplet concentration, and the films no longer upconverted below the glass transition temperature of the polymer.

Similar work suspending molecular sensitizers and emitters in polymers were tried, however, these attempts consistently yielded upconversion efficiencies far below efficiencies in solution.[12-14] These works were primarily done with the intention of

biological applications, and focused on decreasing power densities to limit possible damage to living tissue. Other morphologies explored included nanospheres which encapsulated the organic dyes in glassy polymers, where due to limited volume, increased exciton mobility and led to green to blue upconversion efficiencies around 4%.[15]

Other sensitizers and emitting molecules have also been employed in thin films, such as in 2018 by a South Korean group in ACS Applied Materials and Interfaces. By embedding PdTPBP as sensitizer and perylene as emitter in a rubbery polymer, which was the first report of this specific upconversion system in the solid state.[16] This work focused on flexible upconverting thin films fabricated by spin coating PdTPBP palladium sensitizer and perylene emitter blended together in a polyurethane layer. The resulting film gave an upconversion quantum yield reaching above 3% efficiency (7% when defining QY as 100% when all photons undergo upconversion) with an excitation intensity of 70 mW cm^{-2}. The major benefits of this study were air stability due to oxygen protecting polymer layers and the low excitation density required.

1.6 Conductive polymers

Advances in upconversion efficiencies came from doping conductive polymers, which doubled as both polymer matrixes and effective acceptors. By using this approach, Monkman et al were able to achieve 6% efficiency, however, such conductive polymer materials are quite brittle in the solid state and lack practical widespread adaptability.[17] Separately, Castellano et al sought to overcome the low diffusivity of organic molecules in rigid glassy polymers by employing elastomers (thermoplastic elastomers) where the sensitizer and emitter molecules diffusivity are 5-7 orders of magnitude larger, allowing

for efficiencies of 11% in the solid state.[18] Meinardi's work in 2013 used a similar process, but focused on polyacrylates as their polymer matrix due to ease of polymerization and ability to dope with desired PtOEP and DPA upconversion system.[19] With this system, the Meinardi group was able to measure upconversion before and after polymerization, showing minimal decrease in efficiencies once in the polymerized solid. The solution based system was measured at 22% in the linear regime, and after polymerization fell to only 17%, a feat attributed to the retention of luminescence properties of the emitter in the rubber material and uniformly crosslinked polymer matrix formed.[19] This remains the highest upconversion QY reported in the solid state, however, these polymers still require protection from oxygen which still limits long term stability and usefulness.

Jonas Sandby Lissau et al created a hybrid approach in 2015 which relied on emitters attached to mesoporous ZrO2, however these thin films were sensitized by solution-based sensitizers. The thin films in this study were nanostructured ZrO2 blade-casted on to glass slides with a resulting thickness between 1 and 3 μm. These films were then placed in a cell with a solution of PdOEP as the sensitizer. This hybrid approach, while innovative, is unable to fully remove the solvent and overcome the practical concerns of solution-based systems. This same group reported successful upconversion PdOEP physisorbed onto the ZrO2 thin film, however, with very low efficiency due in part to sensitizer aggregation.[20]

1.7 Perovskite based upconverting thin films

More recent work from the Congreve lab and Lea Nienhaus has focused on perovskites as efficient ligand free thin film sensitizers to a thermally deposited rubrene thin film. This lead halide-based perovskite upconversion system has low efficiency but allows for upconversion with powers achievable below solar flux. The major benefits of using perovskites as sensitizers is their high absorption in the NIR, efficient free carrier generation at room temperature, and lack of insulating surface ligands. Instead of using surface ligands to passivate a nanocrystal surface, thin films of lead halide perovskites were passivated by a thin film of rubrene, which also served as the TTA based emitter. Using these perovskite-based upconversion thin films, Nienhaus produced upconversion starting at 3.1% (normalized to a maximum efficiency of 100%) with incident power more than 80 W/cm^2. Subsequent studies on the thickness of the perovskite layer was able to lower the upconversion threshold down to 7.1 mW/cm^2, a significant improvement and an excitation intensity below that of one sun.

1.8 The future of upconverting thin films

While many groups have successfully fabricated organic based upconverting thin films, the same spectral and power limitations have followed these systems and limit their usefulness. Strong advances have been made using perovskite thin films, however, when low upconversion threshold is desired, upconversion quantum yields suffer. The most promising upconversion in solid state will rely on carefully selected materials, both relying on promising polymer hosts and new upconversion sensitizers that overcome the limited scope of organic porphyrin options. We believe that nanocrystals provide the

opportunity to use the high efficiency exciton transporting polymer hosts with tunable and robust NIR sensitizing materials. As we transition the advantages of organic-nanocrystal hybrid upconversion into thin films, the advances made in these exciting solid state materials can be transitioned to include new non-toxic silicon nanocrystals[21] to produce biocompatible upconversion materials, stepping closer to the full potential of this powerful energy system.

Chapter 2 Primary amines enhance triplet energy transfer from both the band edge and trap state from CdSe nanocrystals

2.1 Introduction

In this study, the role that primary amines play during triplet energy transfer from photoexcited CdSe nanocrystals (NCs) was examined. Colloidally synthesized CdSe NCs were placed in varying concentrations of 1-propyl- or 1-octylamine, with and without 2-anthracenecarboxylic acid transmitter ligands attached. Primary amines have been shown to increase the photoluminescence quantum yield (PLQY) of CdSe nanocrystals (NCs), yet little is known about their effect on energy transfer. It is well known that surface states play a significant role in mediating charge and energy transfer in nanocrystalline materials. Hence, a better understanding and the subsequent ability to control surface states is the key to unlocking the full potential of NCs in energy transfer processes that are important, for example, in photon upconversion. In the past, aliphatic amines have been observed to both enhance and quench NC PL.[7-8] For example, low concentrations of primary amines enhance CdSe NC PL more than secondary and tertiary amines,[22] while higher concentrations of amine quench PL [e.g., when the amine to quantum dots (QD) ratio exceeds 1000].[23] Separately, Kalyuzhny and Murray[24] found that thiols quenched CdSe NCs, while hexadecylamine, pyridine, trioctylphosphine, and trioctylphosphine oxide enhanced the PL of CdSe NCs. In contrast, there have not been any reports on the effect of common ligands on energy transfer.

In this work, we examine the effect of primary amines on triplet energy transfer (TET) that occurs during photon upconversion. Photon upconversion with a NC and organic hybrid system[5] has promising photovoltaic and bioimaging applications.[2-4] This system capitalizes on the synthetically tunable nature of inorganic nanocrystal absorption and emission, as well as their low rates of nonradiative recombination compared to their organic near-infrared (NIR) absorbing counterparts. By transferring spin-triplet excitons from an inorganic CdSe nanocrystal to an organic acceptor, the benefits of strong semiconductor absorption and small exchange splitting can be coupled with the propensity for triplet-triplet annihilation in organic emitters. This photon upconversion system is described in Figure 2.1 (a), where 488 nm CW laser light is absorbed by the CdSe NC sensitizer. Triplet energy transfer (TET, red arrows) then occurs to surface bound 2-anthracenecarboxylic acid (**2-ACA**) and finally to diphenylanthracene (**DPA**) that emits violet light in solution. **DPA** produces this violet light when two molecules in their triplet excited state annihilate (black dotted arrows) to one in the ground state and the other in the first excited state. The latter can radiatively decay and emit photons centered at 430 nm. Figure 2.1 (b) contains the absorption and photoluminescence (PL) spectra of **2-ACA**, **DPA**, and CdSe.

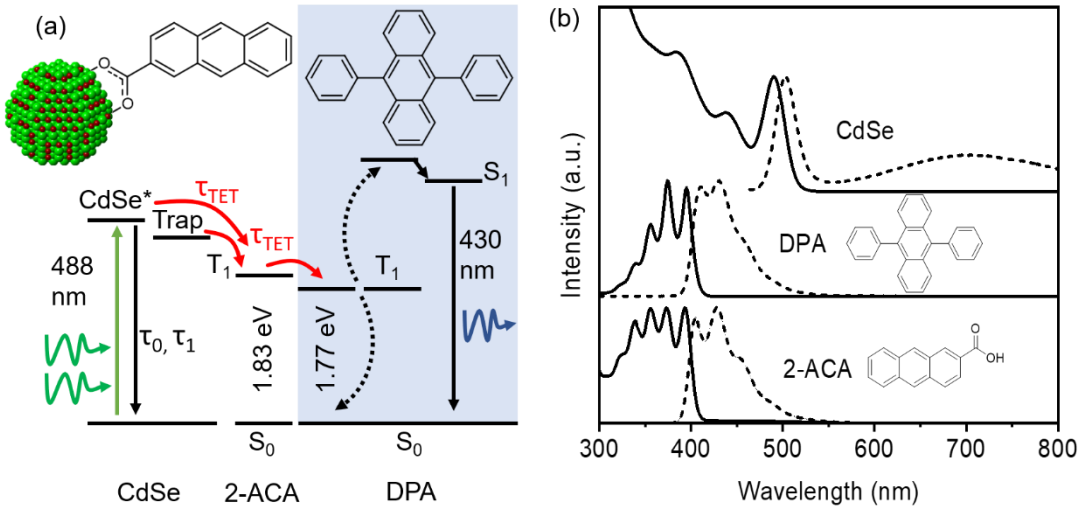

Figure 2.1 (a) Illustration depicting photon upconversion, showing photoexcitation of NCs, triplet energy transfer (TET) to bound 2-anthracene carboxylic acid ligand (2-ACA), TET and triplet-triplet annihilation of the diphenylanthracene (DPA) emitter. (b) Absorption (solid lines) and photoluminescence (dashed lines) of 2-ACA, DPA, and oleic acid functionalized CdSe NCs. Spectra were measured at room temperature, with CdSe and DPA in toluene, and 2-ACA in tetrahydrofuran.

In order to boost upconversion efficiencies, a transmitter ligand is bound to the NC surface to enhance the orbital overlap necessary for Dexter-like energy transfer. Typically, 9-anthracenecarboxylic acid (**9-ACA**) is surface bound, and the **CdSe/9-ACA** hybrid NC/transmitter system can lead to upconversion efficiencies of 15% when mediating energy transfer from CdSe triplet photosensitizers to the **DPA** emitter in solution.[25-26] In contrast, without the **9-ACA** transmitter ligand, photon upconversion QYs are three orders of magnitude lower when CdSe is bound only with the native surfactants. When primary amines were added to **CdSe/9-ACA**, no enhancement was seen [Figure 5.2 (a)]; however, with the **2-ACA** transmitter, the same primary amine, 1-octylamine, enhanced photon upconversion 4–5 times, albeit from a lower photon upconversion QY base level of ~1% **(**Figure 5.2 and Figure 5.7).[26-27] It has proven challenging to differentiate the ligand binding geometry between these **ACA** isomers on

the nanocrystal surface.[28-29] Attenuated total reflection infra-red (ATR-IR) measurements show little difference between isomers, probably because the transmitter ligands make up less than 5%–10% of the total bound molecules on the surface, assuming ~100 oleic acid (OA) ligands per NC.[30-31] Similarly, in our hands, ^{77}Se solution-based nuclear magnetic resonance of the CdSe/ACA hybrid system has not been able to shed light on ligand conformation.

Thus, we turn to transient absorption measurements to provide insight into the role primary amines play in enhancing the photon upconversion QY 4–5 times for the **CdSe/2-ACA** light absorber/transmitter system. We used small CdSe NCs 2.3 nm in diameter with absorption maxima of 490 nm to maximize the driving force for triplet energy transfer. This eliminates back transfer as TET proceeds unilaterally in one direction from NC to transmitter.[32] 1-propylamine (**PA**) was chosen for its ability to penetrate the native ligand shell without being too volatile (like ammonia) or too bulky to sterically block the approach of the **DPA** annihilator during photon upconversion.[33] The amine group is noted for its nucleophilicity and relatively strong binding to cadmium chalcogenide NCs.[30]

In line with previous reports,[7-8, 22-24] here, primary amines enhance CdSe NC band edge and trap state PL. Figure 2.2 (a) shows the absorption and PL of the native oleic acid capped CdSe NCs (**1**, black) in the presence of different concentrations of **PA** (10 mM and 90 mM, samples **2** and **3** in red and brown, respectively). As summarized in Table 2.1, CdSe NCs with native ligands in toluene have trap state PL 3.5 times higher than the band edge PLQY of 0.23%. The ratio of the trap emission PL to the band edge

emission PL decreases from 3.5 to 0.4 as the concentration of primary amine is increased to 90 mM, showing that primary amines enhance band edge fluorescence preferentially over trap emission. Comparing samples **1** to **3**, the addition of **PA** increases the PLQY of the NC at its band edge and trap position 26-fold and 4-fold, respectively. This has previously been attributed to the lone pair of the amines passivating dangling bonds on the NC surface.[7, 24, 30] Note that the increase in PL with amine concentration is superlinear like reported by Owen *et al.*,[30] as reflected in Table 2.1 when comparing between samples **1**, **2**, and **3**.

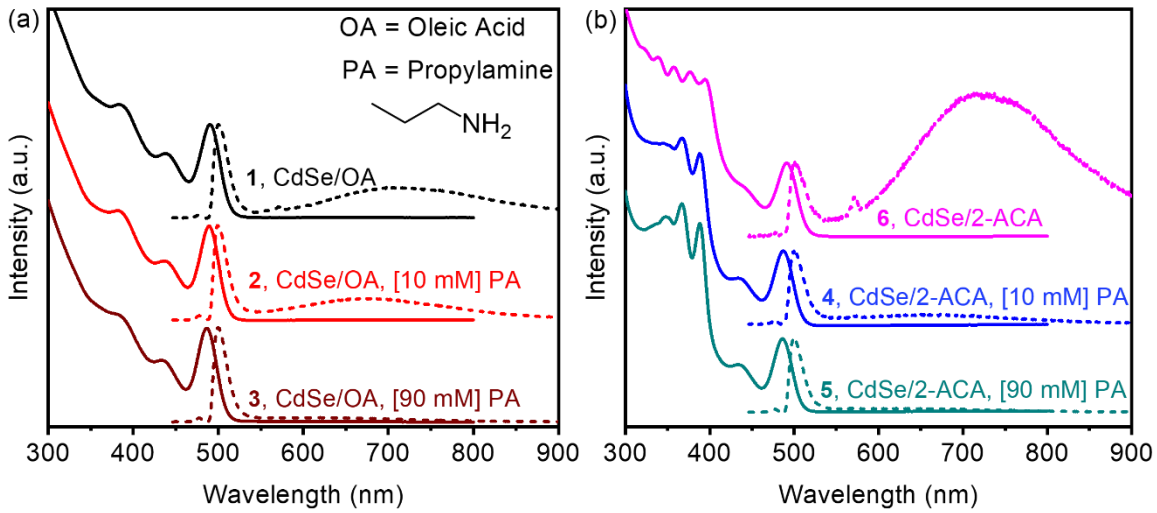

Figure 2.2 Normalized absorption and photoluminescence spectra of 2.3 nm diameter CdSe nanocrystals with (a) native oleic acid (OA) ligands and (b) 2-ACA bound to NC surface in 10 mM and 90 mM propylamine (PA). All measurements were performed at room temperature in toluene.

Table 2.1 The band edge and trap photoluminescence quantum yields (QYs) of CdSe nanocrystals (NCs). Samples 1–3 only have oleic acid (OA), but samples 4–5 have both OA and an average of eight 2-ACA transmitter ligands bound. Photon upconversion QYs in 3 mM diphenylanthracene (DPA). Global fitting parameters of the kinetics at 433 nm from transient absorption for samples 1–5. τ_0, τ_1 are the lifetimes of the decays of the NCs at 433 nm. τ_{N0}, τ_{N1}, τ_{N2}, and τ_{TET} are the perturbation to the lifetimes from PA and TET. All measurements were performed in toluene at room temperature.

CdSe	**1: OA**	**2: OA**	**3: OA**	**4: 2-ACA + OA**	**5: 2-ACA + OA**
Propylamine (mM)	0	10	90	10	90
τ_0 (ns)	11.09	11.09	11.12	11.09	11.12
τ_1 (ns)	0.177	0.177	0.179	0.177	0.180
τ_{N0} (ns)	…	−36.3	0.294	0.296	0.239
τ_{N1} (ns)	…	−1.55	0.0269	0.0200	0.0188
τ_{N2a} (ns)	…	…	12.9 ± 0.4	…	…
τ_{TET} (ns)	…	…	…	6.57 ± 0.12	4.94 ± 0.17
PLQY (%)	0.23	2.01	5.96	0.68	1.60
Trap QY (%)	0.80	4.33	2.35	0.71	0.68
Upconversion QY (%)	0	0	0	2.89	2.71
Φ_{TET} (%)	…	…	…	1.18	1.57

When the CdSe NCs are functionalized with **2-ACA**, the photon upconversion QY increases by up to 4.4 times in the presence of **PA** (samples **4** and **5**, Table 2.1). **CdSe/2-ACA** has a band edge, trap state, and photon upconversion PLQY of 0.02%, 0.36% and 0.65%, respectively. In the presence of amine, the band edge PL increases up to 80-fold and trap PL doubles, as shown in Table 2.1. Figure 2.2 (b) shows the same CdSe nanoparticles with an average of eight **2-ACA** ligands bound to the surface in the same two concentrations of **PA** as before (**4** and **5**, blue and teal, respectively) and in pure toluene only (**6**, magenta). This transmitter loading gave the highest photon upconversion QYs for this hybrid system in the presence of 3 mM **DPA** in toluene (Table 2.1). Though photon upconversion is maximized at low (10 mM) concentrations of propylamine, the PLQY is further enhanced with increasing primary amine concentration. When comparing the CdSe PLQY with the same concentrations of amine, the presence of **2-ACA** quenches the 10 mM and 90 mM amine samples 66% and 73% at the band edge and the trap state 84% and 85%, respectively. This quenching of both the band edge and the trap emission suggests that the presence of the **2-ACA** transmitter invites triplet energy transfer from excitons pinned at both states.

To study the excitonic pathways populated in the presence of amine, ultrafast transient absorption measurements were employed to track excited state dynamics in a 3 ns window. Excitation at 490 nm means that only the CdSe NC is excited, similar to our photon upconversion experiments. Figure 2.3 shows representative TA spectra of samples **2–5**, while Figure 2.4 (a) shows the trajectory of the original photoexcited oleic acid capped CdSe NCs (**CdSe/OA**, sample **1**). The positive features in each spectrum

were assigned to excited state absorption (ESA). The negative features are the ground state bleaches (GSB) which correspond to peak maxima in the linear absorption spectra of the NC (plotted in black above every TA trace). As shown in Figure 2.4 (a), sample **1**, **CdSe/OA**, has an isosbestic point at 420 nm. Thus, any change at 420 nm is due to the presence of the **PA** or **2-ACA** transmitter. To extract the triplet energy transfer term, time traces at 420 nm for **CdSe/2-ACA** in the presence and absence of [10 mM] and [90 mM] **PA** were compared [Figure 2.4 (b)]. Double difference traces at 420 nm subtracting **2** from **4** and **3** from **5** (where **2** = **CdSe/OA** [10 mM] **PA** and **4** = **CdSe/2-ACA** [10 mM] **PA**; while **3** = **CdSe/OA** [90 mM] **PA** and **5** = **CdSe/2-ACA** [90 mM] **PA**) were fit with a single exponential decay. The resulting decay constant corresponds to the rate of triplet energy transfer. As shown in Table 2.2, samples **4** and **5** have a TET lifetime of 6.6 and 4.9 ns, respectively, which is expected considering the large driving force and the photon upconversion QY of about 3%. Previously, we measured an average rate of TET of 0.63×10^6 s^{-1} for CdSe/**2-ACA** without amine. The rates of TET here of $(152–202) \times 10^6$ s^{-1} for samples **4** and **5** are substantially faster. However, we note that our previous report used a stretched exponential to obtain the average rate of TET, a substantially different analysis. Stretched exponentials give an average decay rate that is difficult to assign to a physical process. In contrast, the high-quality data obtained here allow more careful analysis.

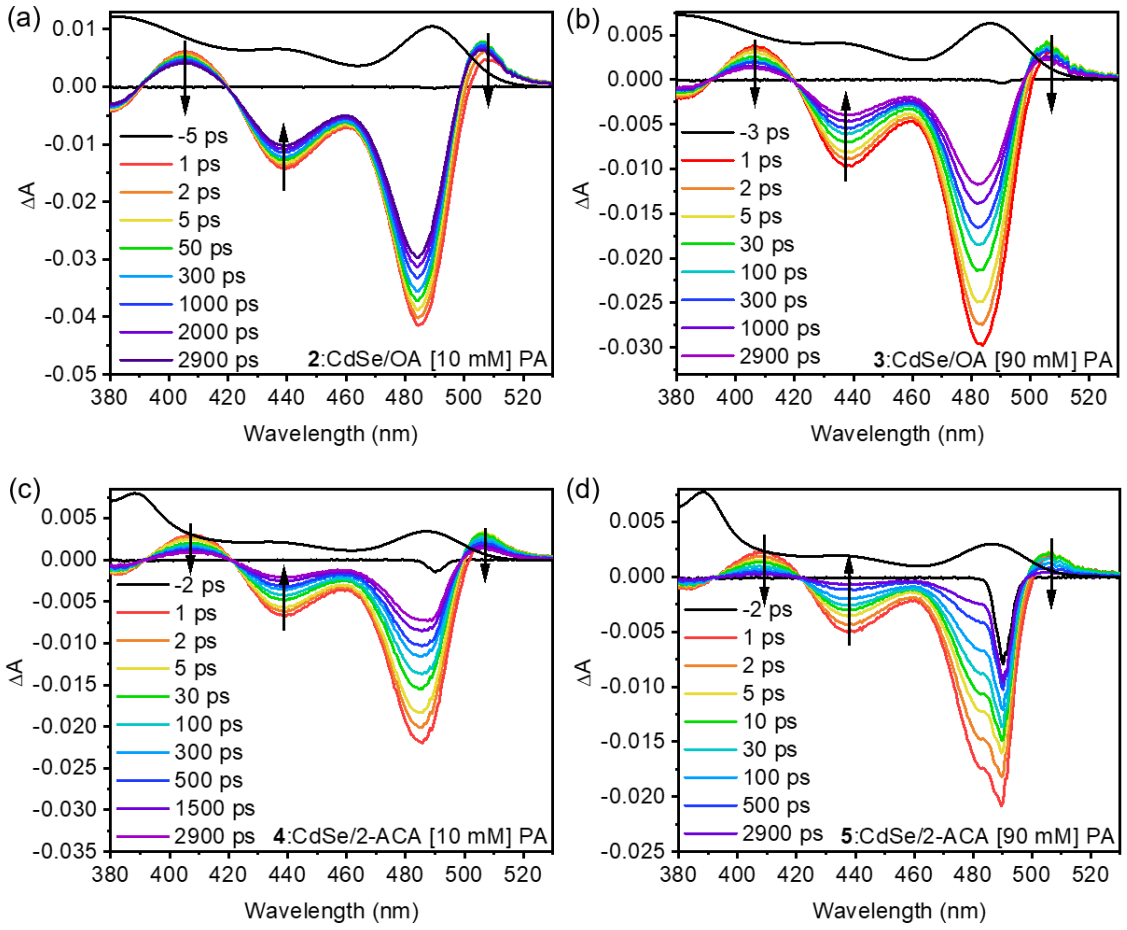

Figure 2.3 Transient absorption spectra of (a) sample 2, (b) sample 3, (c) sample 4, and (d) sample 5, all measured following excitation at 490 nm, with steady state absorption spectra shown above. All spectra were recorded of samples in inert environment at room temperature.

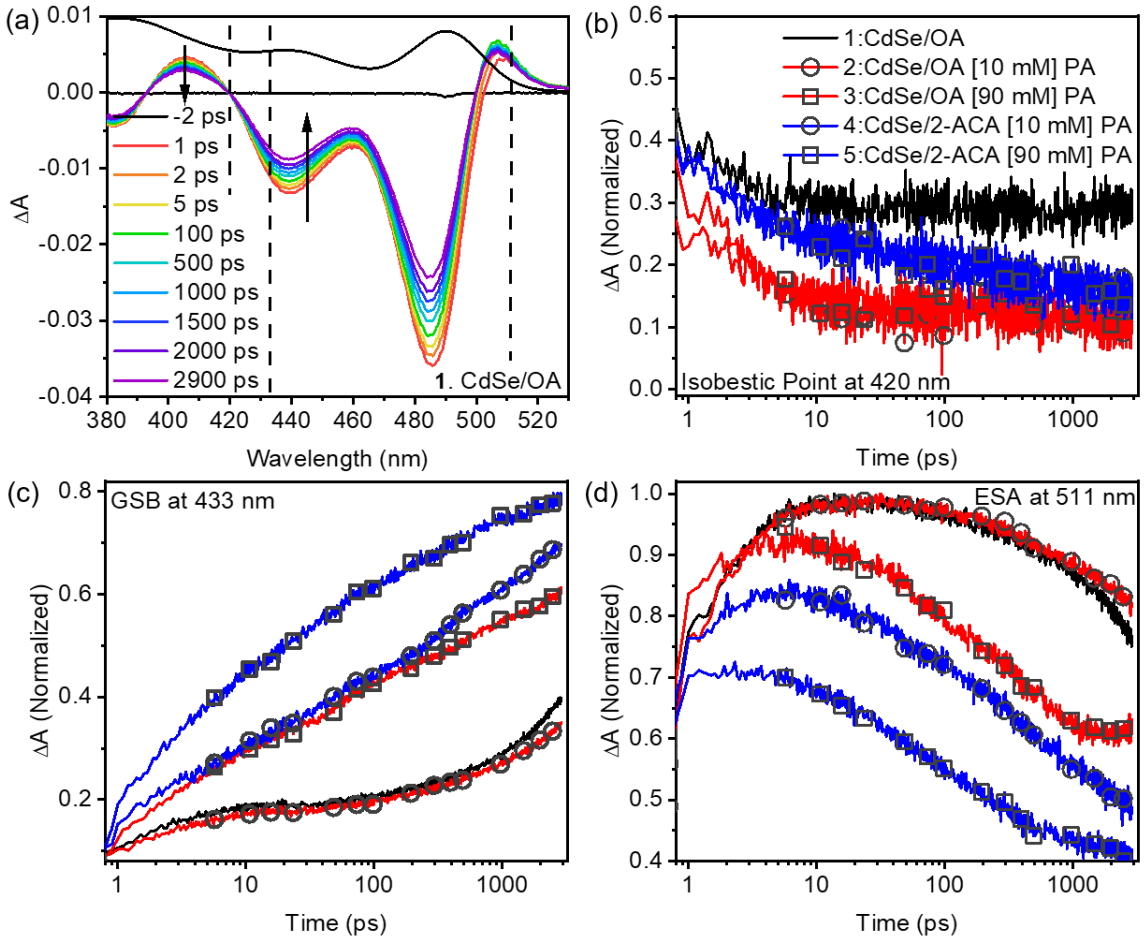

Figure 2.4 (a) Transient absorption spectra of sample 1, with steady state absorption spectra shown above and 420 nm, 433 nm, and 511 nm marked. (b) Transient absorption traces at the isosbestic point (420 nm) showing contribution of TET to bound 2-ACA in samples 2 and 3. (c) Ground state recovery (GSB) at 433 nm, illustrating relative quenching of CdSe NC in the presence of both surface-bound 2-ACA and high concentrations of amine. (d) Excited state absorption (ESA) at 511 nm corresponding to the trap state.

Table 2.2 Global fitting parameters for the kinetics of the trap state, measured at 511 nm for samples 1–5 from transient absorption. τ0, τ1 are the lifetimes of the decays of the NCs at 511 nm. τN0, τN1, and τN2, are the corresponding perturbation to the lifetimes from the contribution of the amine and TET.

CdSe	***1: OA***	***2: OA***	***3: OA***	***4: 2-ACA + OA***	***5: 2-ACA + OA***
Propylamine (mM)	0	10	90	10	90
τ_0 *(ns)*	13.1	13.1	13.1	13.1	13.1
τ_1 *(ns)*	0.365	0.365	0.365	0.365	0.365
τ_{N0} *(ns)*	…	0.669	−39.4	8.73	3.83
τ_{N1} *(ns)*	…	−0.369	0.432	0.217	0.112

The amine increases CdSe NC PL first by decreasing nonradiative loss processes at low concentrations, then by enhancing radiative pathways at higher concentrations. This is inferred from both the TA spectra and steady-state PLQY measurements (Table 2.1) of CdSe NCs capped with only oleic acid (samples **1–3**). When small amounts of amine are added to the NC (10 mM), as in sample **2**, the band edge PLQY is enhanced 8.7 times compared to the native NC (sample **1**). However, the recovery of the GSB at 433 nm and ESA at 511 nm remains unchanged, as shown in Figure 2.4 (c) and Figure 2.4 (d), where the red and black traces virtually overlap. This suggests that small amounts of amine effectively decrease the nonradiative rate of the NC. When the amine concentration is raised to 90 mM, as in sample **3**, an additional fast decay component is observed in the 3 ns time window (black squares on red line) in tandem with a 26-fold increase in the band edge PL compared to the native CdSe NCs (sample **1**). A similar situation occurs when **2-ACA** is bound onto the surface of CdSe [blue traces in Figure 2.4 (c) or Figure 2.4 (d)], where large amounts of amine deplete the excited state faster,

resulting in more PL at both the band edge and trap state. Since radiative lifetimes of CdSe NCs are on the order of 10s of nanoseconds,[34-36] we realize that our 3 ns window does not fully capture the entire radiative decay, but it does provide insight into how the branching ratios of the excited state are diverted in favor of radiative processes in the presence of amine.

When transmitter ligands are added to the surface of the NC, the PLQY at the band edge and trap state is reduced by about 3- to 6-fold, as seen when comparing samples **4** and **5** to samples **1** and **2** where CdSe only has **OA** on its surface. To examine this further, we globally fit the kinetics at 511 nm which represents the broad trap state [Figure 2.4 (d)]. Two intrinsic decay constants of τ_0 and τ_1 of 13.1 ns and 0.37 ns are observed in all samples. Samples **1** and **2** look identical as their spectra in Figure 2.4 (d) would suggest. However, in the presence of excess amine (sample 3), **CdSe/OA's** trap state is rapidly depopulated by an additional 39.4 ns component. This is commensurate with a decrease in trap state emission and increase in band edge PL compared to sample **2** (less amine) and can be explained by an energetically shallow trap state that allows the NC exciton to shuttle back to the band edge. In the presence of the **2-ACA** ligand, additional time constants of 8.73 ns and 3.83 ns deplete the trap state in samples **4** and **5**, respectively. This compares well to τ_{TET} of 6.6 ns and 4.9 ns extracted independently from the isosbestic point at 420 nm and suggests that this broad trap state participates in triplet energy transfer to surface bound **2-ACA** and is thus depleted in the presence of the transmitter ligand.

Using the TET rate from the isosbestic point at 420 nm, the decay of the exciton bleach of CdSe NCs for all samples was globally fit to obtain the intrinsic decay amplitude and time constants of QD excitons and the amplitude of the triplet energy transfer component. Some of the key fitting parameters are listed in Table 2.1 and Table 2.2 (see Chapter 5 Supporting Information for the quality of the fits). Two decay components, τ_0 and τ_1 of 11.1 ns and 0.18 ns, respectively, were needed to fit the original CdSe NCs globally [Equation (5.1)]. The presence of 10 mM **PA** (sample **2**) introduces additional time constants of $\tau_{N0} = -36.3$ ns and $\tau_{N1} = -1.55$ ns that effectively slow the intrinsic decay of the CdSe NC's τ_0 and τ_1, respectively [Equation (5.3)]. This, in combination with an 8-fold increase in steady state PL at the band edge, suggests that small concentrations of amine suppress the nonradiative rate of the NC. With more **PA** at 90 mM in sample **3**, the exciton is preferentially steered toward fluorescent pathways, with an additional decay channel opening ($\tau_{N2} = 12.9$ ns). When CdSe is only functionalized with oleic acid, 82%–95% of the exciton decays with 11–13 ns time constants.

2.2 Conclusion

When CdSe NCs are functionalized with **2-ACA**, the global fit at 433 nm reveals that a third to half of the excited state contributes to triplet energy transfer. In samples **4** and **5**, the 433 nm wavelength includes the T_1-T_n transition of the bound **2-ACA** that is observed after triplet energy transfer from the photoexcited CdSe NCs to the bound ligand[37]. This broad T_1-T_n transition is a positive feature in the TA spectra, and its growth would appear to add to the recovery of the GSB of the CdSe. When both **2-**

ACA and amine are present, the exciton recovers faster due to both triplet energy transfer and enhanced radiative decay. In these samples with the transmitter ligand, the native nanocrystal decay is dominated by triplet energy transfer (TET) to the **2-ACA**, with weights of 56% and 33% (see A_2 in Table 2.2) to τ_{TET} for samples **4** and **5**, respectively [Equation (5.5) in Chapter 5 Supporting Information]. Comparing samples **4** and **5**, although the presence of additional amine speeds up TET, it also enhances PL from the band edge, resulting in no significant improvement in the photon upconversion QY overall.

Finally, we have shown that primary amines increase the photon upconversion QY with a **CdSe/2-ACA/DPA** photosensitizer/transmitter/emitter system about 5-fold. Transient absorption measurements show that propylamine enhances triplet energy transfer by two ways. First, it decreases the contribution of the nonradiative decay processes in the CdSe NC. Second, it increases the rate of triplet energy transfer. Analysis of the kinetics of the broad surface trap state suggests that it also participates in triplet photosensitization, perhaps by equilibrating with the band edge excitons. Since structural information regarding the amine-nanocrystal adduct that improves the photon upconversion QY is elusive, this work allows for a better understanding of the role surface states play in energy transfer. These observations offer a practical route toward optimizing hybrid organic-inorganic energy harvesting platforms.

Chapter 3 On the size-dependence of CdSe nanocrystals for photon upconversion with anthracene

3.1 Introduction

In triplet-triplet annihilation (TTA) based photon upconversion, controlling triplet energy transfer (TET) through the system is key to unlocking higher efficiencies. In this work, we vary the size of colloidally synthesized CdSe nanocrystals (NC) to examine the effects on TET during photon upconversion, using steady-state measurements and transient absorption spectroscopy. As CdSe NC size increases, the photon upconversion quantum yield (QY) decreases due to the decrease in the rate of TET from CdSe to the surface bound anthracene transmitter ligand, as expected for the Marcus description of energy transfer from the transmitter to the NC. Long microsecond transmitter lifetimes are critical to high photon upconversion QYs.

Triplet-triplet annihilation (TTA) based upconversion systems show great promise for use in efficient photovoltaic and bioimaging technologies. While purely organic TTA upconversion systems rely on finding new sensitizers for every wavelength of interest, inorganic nanocrystals (NCs) are widely tunable sensitizing materials with robust absorption and emission properties. In addition to tunability, NCs can have low rates of nonradiative recombination in spectral areas of interest such as the NIR. By combining the strong absorption and small exchange splitting of inorganic nanocrystals with existing organic TTA materials, we can design robust and flexible upconversion systems if all the elementary steps in triplet energy transfer are understood.[5] Ultimately, these systems will

allow the size and composition of quantum dots to be varied to select for the absorption of desired wavelengths of light, providing an optimum design path for efficient upconversion systems with diverse applications.[2-5]

In the model system studied here, CdSe NC photosensitizers absorb 532 nm light from a continuous wave laser (Figure 3.1a). This energy then transfers to the spin-triplet excited state of a bound 9-anthracene carboxylic acid (**9-ACA**) transmitter ligand. A second triplet energy transfer (TET) step may occur to diphenylanthracene (**DPA**) emitter molecules, where two neighboring **DPA** in their triplet excited states combine via spin allowed TTA (black dotted arrows) to produce one in the singlet excited state (S_1) and one in the ground state (S_0). The newly populated singlet state can then emit violet light centered at 430 nm in solution. Because triplet-triplet annihilation and fluorescence are intrinsic properties of the emitter molecule, this work focuses on elucidating the bottlenecks hindering triplet energy transfer from the NC donor to bound 9-ACA ligand, and subsequently to the **DPA** emitter (TET1 and TET2 in Fig. 1a). Our steady-state photon upconversion experiments and transient absorption (TA) spectroscopy reveal that TET1 is in the Marcus normal regime.[38-39] The efficiency of the first TET step, Φ_{TET1}, is as high as 85% for small QDs[40] due to the large driving force but decreases for larger particles. In contrast, Φ_{TET2} is quantitative for small NCs but small for large CdSe QDs. TA measurements show that this is because smaller NCs support long 9-ACA transmitter lifetimes on the order of hundreds of μs, whereas 9-ACA has short ~18 ns lifetimes on large nanoparticles, decreasing Φ_{TET2}.

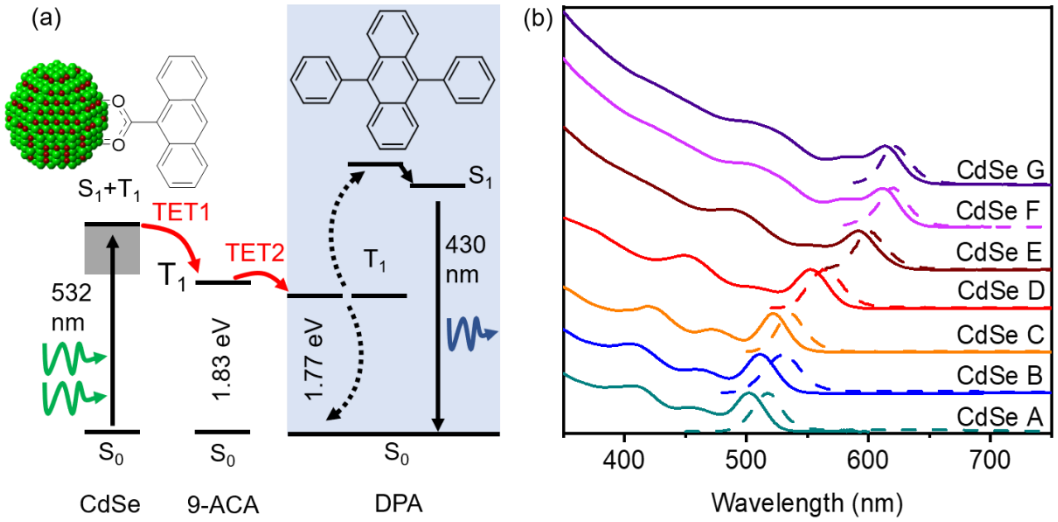

Figure 3.1 (a) Energy diagram depicting photon upconversion, showing photoexcitation of CdSe nanocrystals, triplet energy transfer (TET) TET1 to bound 9-anthracene carboxylic acid transmitter ligand (9-ACA), and TET2 to the diphenylanthracene (DPA) emitter. (b) Normalized absorption (solid lines) and photoluminescence (dashed lines) spectra of seven zb-CdSe nanocrystals dispersed in toluene. 505 nm CdSe is reprinted from ref [9] with permission.

Several zb-CdSe nanocrystals (NC) were synthesized with diameters ranging from 2.4-5.3 nm. Figure 3.1b contains the absorption (solid lines) and emission (dashed lines) spectra of all seven CdSe explored in this work (A-G). This range of CdSe NCs was chosen for DPA triplet photosensitization. Considering that DPA's lowest excited triplet state is at 1.8 eV, and the CdSe NC bandgap here varies from 2.45-2.02 eV, the driving force for TET1 here ranges from 0.65-0.22 eV. Smaller CdSe NCs can be synthesized, however these small particles exhibit lower stability (increased ripening) and begin to absorb in the same region as the DPA emitter, detracting from the goal of photon upconversion. The NCs were functionalized with 9-ACA ligand and re-dispersed in 3 mM DPA for photon upconversion (see details in the Supporting Information) with 532 nm cw light. In terms of photon upconversion, larger CdSe NC required higher ligand surface densities than their

smaller NC's counterparts. Like has been shown previously,[40-41] there is an optimal 9-ACA surface density that results in a maximum photon upconversion quantum yield (QY), where too few 9-ACA transmitter ligands limit TET, and too many result in ligand stacking and excimer formation, providing loss pathways for TET (Fig. S1 shows this ligand optimization). Table 3.1 shows the NC size, absorption, and photoluminescence (PL) maxima (λ_{ABS} and λ_{ABS} respectively); PL QY, Φ_{PL}; average number of surface bound 9-ACA ligands, n; as well as the surface density of this transmitter molecule. Equation S1 gives the upconversion QYs in Table 3.1 (out of a 100%). The small particles A and B have high photon upconversion QYs, Φ_{UP} of about 12-16%. Φ_{UP} drops to ~8-10% for mid-sized CdSe NCs that absorb strongly in the green, while larger CdSe NCs that absorb to the red of 600nm suffer from low Φ_{UP} ~ 0.4-1.7%.

Table 3.1 Key Parameters of CdSe NCs used in upconversion and TA experiments.

CdSe NC radius (nm)	λ_{ABS} (nm)	λ_{PL} (nm)	CdSe NC Φ_{PL} (%)	Φ_{UP} (%)	n (9-ACA/ CdSe NC)[a]	9-ACA Density[b]	k_{TET1} (ns^{-1})[c]
A*	1.20	505	520	2.1	12.7	7.4	0.409	59.8
B	1.23	511	529	29.2	15.8	8.4	0.443	15.2
C	1.27	523	536	18.7	10.0	5.2	0.257	8.89×10^{-3}
D	1.54	552	562	18.6	8.5	15.3	0.515	1.86×10^{-4}
E	2.11	591	602	14.9	1.7	36.6	0.657	1.22×10^{-4}
F	2.58	612	620	5.3	0.4	65.1	0.777	5.65×10^{-5}
G	2.66	615	620	6.6	1.0	22.5	0.253	6.74×10^{-5}

[a]The average number of molecules per QD, obtained from UV-Vis absorption spectra in Figure 3.1b and extinction coefficient in Table 5.1. [b]Units of (n/nm^2). [c]Total rate of TET (not normalized by n). [*]Data reprinted from ref [42] with permission.

In order to study the rates of triplet energy transfer, TA spectra were acquired for each NC with 9-ACA attached to the surface at the ligand loading where Φ_{UP} was previously maximized, but without any DPA present. Ultrafast TA spectra were acquired

with each CdSe NC excited at its band-edge to obtain kTET1. As shown in Fig. 1a, kTET1 describes the rate of TET from the CdSe NC to the bound 9-ACA transmitter ligand. Figure 3.2 shows the ultrafast TA spectra of a small sized CdSe C (Fig. 2a) and large sized CdSe G (Fig. 2b) with the CdSe NC ground state bleach (GSB) at its absorption maxima and the triplet excited state absorption (ESA) of 9-ACA marked with vertical dotted lines. (Ultrafast TA spectra of the other CdSe/9-ACA samples B, C, D, E, F, and G are in Figure 5.7). Global fits of the TA data were used to extract the average rate of triplet energy transfer, kTET1, from these six CdSe NCs to the bound 9-ACA ligands. The recovery of the CdSe GSB was analyzed 30 nm blue of the excitation wavelength at the second GSB minima to avoid scattering contribution from the pump. The CdSe GSB was globally fit with the kinetics at 435 nm, which included contributions from the ESA of the 9-ACA T_1-T_n transition and the CdSe NC donor. The trajectory of the CdSe GSB has been fit using equation (1), using two exponentials, and the ESA kinetics globally fit with an additional term to describe kTET1 (see SI section 2, Fig. S3):

$$I(t) = \Sigma_{i=1}^{2} A_i \, exp(-\frac{t - t_0}{\tau_i}) \tag{3.1}$$

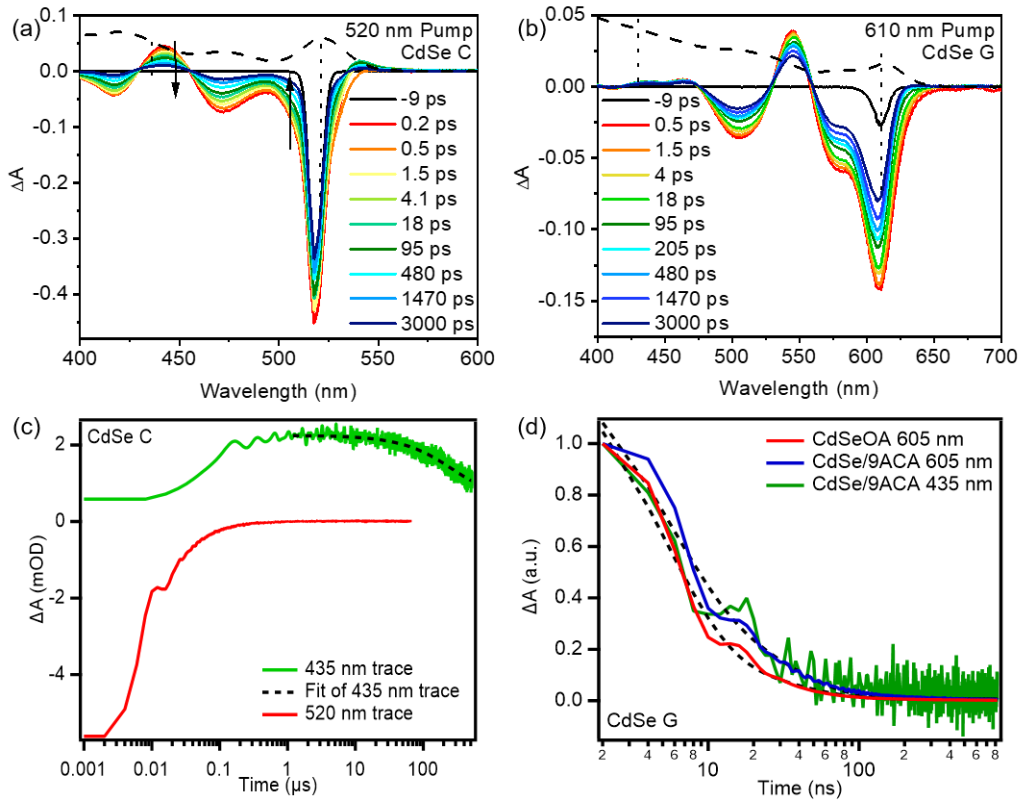

Figure 3.2 Ultrafast transient absorption (TA) spectra of 523 nm (a) and 615 nm absorbing (b) CdSe zb nanocrystals C and G. Vertical dotted lines show ground state bleach (GSB) of CdSe NC's and 435 nm excited state absorption (ESA) corresponding to the growth of the 9-anthracene carboxylic acid triplet. The absorption of CdSe C and G is plotted in broken black lines. Nanosecond TA gives the kinetics at selected wavelengths at (c) 520 nm for CdSe C, (d) 605 nm for CdSe G with native oleic acid ligands only (CdSeOA, red), transmitter ligands (CdSe/9ACA, blue) and 9ACA triplet ESA (green, 10X), and their corresponding fits (black dotted lines).

Global fittings of the GSB and ESA are performed with the linked parameters of t_0 and τ_i. The fitting results and parameters are shown in Table 5.4. The results are summarized in Table 3.1, which shows that kTET1 decreases as CdSe size increases, corresponding to a decrease in upconversion QY. As the driving force for TET1 decreases from 0.65 eV for the smallest CdSe to 0.22 eV for the largest CdSe NCs, kTET1 decreases from 59.8 ns^{-1} to 0.0674 μs^{-1}. The data here suggests that TET1 is squarely in the Marcus normal regime.

Nanosecond TA measurements were conducted to extract the transmitter triplet lifetime, i.e. the 9-ACA lifetime when bound to NC's. We had previously obtained this data for CdSe A, the smallest NC.[40] To obtain these parameters for the midsized and large CdSe NCs, CdSe C and G were excited with 532 nm nanosecond pulses and the kinetics at 435nm and the CdSe GSB were collected (Fig. 2c and 2d). As shown in Fig. 2c, the GSB of CdSe C completely recovers in <100 ns, but the triplet ESA at 435 nm is shows a decay constant up to 500 μs. When bound on mid-sized CdSe C, the decay of this long-lived 9-ACA exciton absorbing at 435 nm can be fit monoexponentially to give a 260 ± 7.8 μs triplet lifetime (Figure 3.2c). This shows that spin-orbit coupling with the CdSe lattice does not strongly impact the anthracene's triplet excited state, unlike tetracene's markedly shortened triplet lifetime when bound on PbS NCs.[42] In contrast, the ESA at 435 nm corresponding to the 9-ACA triplet was very short-lived for the large CdSe-G NCs. This can be rationalized from the lowest excited triplet energy levels of 9-ACA and CdSe G absorption maxima (1.83 and 2.02 eV respectively) being relatively close. This results in barrierless downhill forward energy transfer, and thermally activated back energy transfer between large CdSe NCs and anthracene triplet excitons. Evidence for this hypothesis can be seen in the longer CdSe-G exciton lifetime in the presence of 9-ACA. The intensity weighted lifetime of CdSe-G NCs with and without 9-ACA, $\tau_{G\text{-}AN}$ and τ_G respectively, decreases from 25.3 ns to 17.9 ns, as monitored by the recovery of the CdSe NC's ground state bleach at 605 nm, excited at 532nm, measured with ns-TA (Fig. 2d). A similar trend is observed with the amplitude weighted lifetime (

Table 5.5). Using τ_G, $\tau_{G\text{-}AN}$ and the intrinsic lifetime of surface bound anthracene, τ_{AN} = 260 μs from CdSe-C, we can calculate the 9-ACA triplet lifetime when bound on CdSe-G, $\tau_{AN\text{-}G}$ using the set of coupled rate equations[43-44] governing equilibrium in this system:

$$k_{TET1} = \frac{k_G(\tau_{G-AN}^{-1} + \tau_{AN-G}^{-1} - k_G) - \tau_{G-AN}^{-1}\tau_{AN-G}^{-1}}{k_G - k_{AN}} \quad (3.2)$$

$$k_{backTET1} = \frac{-k_{AN}(\tau_{G-AN}^{-1}+\tau_{AN-G}^{-1}-k_{AN})+\tau_{G-AN}^{-1}\tau_{AN-G}^{-1}}{k_G-k_{AN}} \quad (3.3)$$

Solving equation 2 and 3 using ns-TA data gives k_{TET1} = 0.068 μs^{-1} (close to the value of 0.0674 μs^{-1} in Table 3.1 from ps-TA analysis), a backwards TET rate from 9-ACA to CdSe-G, $k_{backTET1}$, of 39.7 μs^{-1} and $\tau_{AN\text{-}G}$, the 9-ACA lifetime on CdSe-G of 17.8 ns. $k_{backTET1}$ can be expressed through a simple Boltzmann approximation, relating $k_{backTET1}$ to $k^0_{backTET1}$ expressed as:

$$k_{backTET1} = k^0_{backTET1} exp\left(\frac{\Delta E}{k_b T}\right) \quad (3.4)$$

where ΔE is the difference between CdSe-G and 9-ACA triplet exciton energy levels. From equation 4, taking into the account the Stokes shift in the NC PL that would lower the driving force or ΔE (the energy gap between the CdSe donor and the 9-ACA acceptor), we can calculate $k^0_{backTET1}$ should be on the same order of magnitude as $k_{backTET1}$. The fact that equation 2 and 3 gives a value of $k^0_{backTET1}$ 3 orders of magnitude higher than k_{TET1} might initially suggest that the principle of detailed balance does not hold here. However, this may be rationalized by the fact that the density of triplet acceptor states on CdSe NCs is

larger than 9-ACA due to its rich band structure. In addition, NC trap states have been implicated in triplet energy transfer from 9-ACA,[9, 45-46] and in-gap trap states in CdSe-G might serve as a thermodynamic sink for 9-ACA triplet excitons.

Unlike the case of pyrene functionalized NCs that exhibited thermal re-population of CdSe photoluminescence from pyrene,[47] the presence of surface bound 9-ACA does not significantly lengthen the CdSe lifetime.[48-50] All our 9-ACA functionalized CdSe NCs here showed NC excitonic states of the order of tens of ns, in line with previous reports in literature (Table 5.4).[51-54] Considering that the 9-ACA ligand density on the CdSe NC's surface here (0.25-0.66 9-ACA/nm^2) and for the CdSe/pyrene work are about the same, and the propensity for pyrene to form excimers, perhaps it is the pyrene excimer exciton and not the triplet exciton that equilibrates with the CdSe NC's band edge exciton and thus increases the particle lifetime.[47]

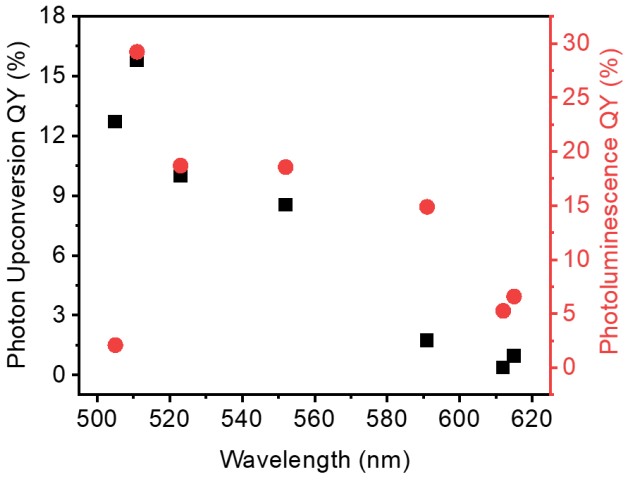

Figure 3.3 (a) The photoluminescence quantum yield (PLQY, red circles) and photon upconversion QY (black squares) of seven zb CdSe nanocrystals (NCs) in toluene using R6G in ethanol as the fluorescence standard plotted versus wavelength of the first absorption maxima of each NC.

3.2 Conclusion

To conclude, we have looked deeper into the first triplet energy transfer step in TTA based upconversion systems to identify where further optimization is needed to increase transition efficiencies. Through static fluorescence upconversion experiments and TA spectroscopy, we have shown that the first TET step is strongly correlated with NC size. Smaller NCs have a larger rate of TET, resulting from a larger driving force. It is demonstrated for small NC systems, both TETs contribute efficiently to the upconversion quantum yield for CdSe/TTA hybrid systems. The variation in photon upconversion and PLQY with CdSe NC size is illustrated in Figure 3.3. Based on these results, we believe the future of efficient energy transfer in quantum dot systems will revolve around finding ways to lengthen transmitter triplet state lifetimes[55] to increase the probability of efficient energy transfer in this complex system.

Chapter 4 High Performing Nanocrystal Sensitized Solid-State Triplet-Triplet Annihilation Based Photon Upconversion

4.1 Introduction

Photon upconversion with a hybrid nanocrystal organic system[4] has promising photovoltaic and bioimaging applications[5, 56-58]. This system capitalizes on the synthetically tunable nature of inorganic nanocrystal absorption and emission, as well as their low rates of nonradiative recombination compared to their organic near-infrared (NIR) absorbing counterparts. By transferring spin-triplet excitons from an inorganic CdSe nanocrystal to an organic acceptor, the benefits of strong semiconductor absorption and small exchange splitting can be coupled with the ability for triplet-triplet annihilation and subsequent fluorescence from organic emitters. This nanocrystal based upconversion system is described in Figure 4.1a where 532 nm CW laser light is absorbed by the CdSe NC sensitizer (black arrow), then triplet energy transferred (**TET**) to the bound transmitter ligand, and **TET** again to the diphenylanthracene (**DPA**). DPA can then undergo triplet triplet annihilation (**TTA**) to create an emissive singlet, giving off violet 430 nm light. This **TTA** process occurs when two excited DPA molecules annihilate to form one DPA in a singlet excited state and one in the ground state. In this work, we focus on photon upconversion in the thin film architectures depicted in Figure 4.1b, a blended film with all components mixed, and a layered film where the CdSe NCs are separated from the DPA in two layers. Figure 4.1c shows the absorption (solid lines) and emission (dashed lines) of

both the CdSe absorber with bound transmitter 9-ACA ligand and DPA emitter for this system.

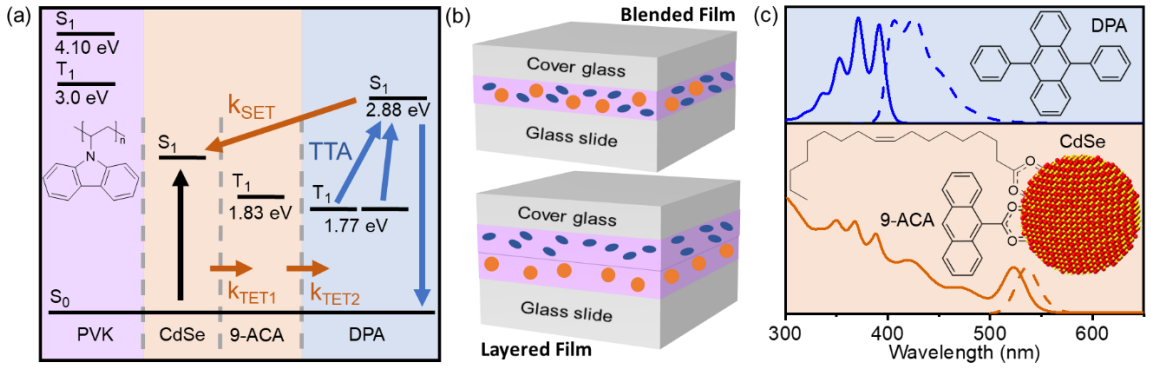

Figure 4.1 (a) Energy diagram illustration depicting photon upconversion, showing photoexcitation of NCs, triplet energy transfer (TET1) to bound 9-anthracene carboxylic acid ligand (**9-ACA**), TET2 to triplet-triplet annihilation diphenylanthracene (**DPA**) emitter. (b) Cartoons of blended (top) and layered (bottom) thin film morphologies. (c) Normalized absorbance (solid lines) and fluorescent (dashed lines) emission spectra of seven zb CdSe nanocrystals dispersed in toluene.

Much work has been done in the past to turn these solution-based upconversion systems into solid-state materials, however, the resulting reports suffer from upconversion efficiencies that are typically much lower than those reported in solution. This is typically due to decreased triplet mobility in rigid systems and increased aggregation of the sensitizer and molecular emitter. Previous work on DPA-decorated supramolecular gels has focused on forming an annihilator decorated polymer matrix which then could be doped with sensitizer in order to preserve efficient triplet energy transfer.[43, 59] Other groups have tried to dope a palladium porphyrin sensitizer directly into an emissive copolymer host capable of TTA for upconversion which resulted in efficiencies of up to 6% out of a possible 50%.[17] The lack of variety in sensitizers, however, leads to very limited viability when looking forward to robust applications in the near-infrared.

Here, we have transformed a solution-based CdSe NC-based hybrid system that can convert green light to violet light relatively efficiently with QYs of over 20%[6, 60-61] (out of 100%) into a solid-state upconverting material for the first time. This. In this work, we have chosen the wide-bandgap polymer poly(9-vinylcarbazole) (PVK) to form a polymer host matrix for both sensitizer and emitter components. This phosphorescent PVK polymer host material is commonly used in OLEDs and has demonstrated efficient triplet exciton fusion for upconversion based light-emitting diodes.[62] Phosphorescent polymer hosts preserve emission primarily from their dopant molecules (in this case, DPA). The rigid PVK host facilitates singlet PL decay from DPA, making PVK an ideal host for our TTA based upconversion system.

We chose two different thin film morphologies to study, a blended morphology where both sensitizer and emitter are well-dispersed in the same PVK polymer layer, and a layered morphology where sensitizer and emitter are in separate layers (Figure 4.1c). In principle, the layered morphology could help prevent Förster resonance energy transfer (FRET) from the DPA emitter to the CdSe NCs, this minimizing parasitic reabsorption. For the blended film, the thin film fabrication process started with dissolving PVK and DPA (20 wt%) in 1,2-dichlorobenzene (*o*-DCB) then adding 532 nm absorbing CdSe nanocrystals functionalized with 9-ACA transmitter ligands (see SI for ligand exchange procedure and optimization, Figure 5.9). The layered morphology solutions were prepared similarly, but the difference is that separate PVK solutions for the CdSe and DPA were made instead. Once fully dissolved, a consistent volume of polymer solution was drop casted onto uniform glass coverslips using volumetric pipettes. After annealing at 60 ˚C

for ten minutes the films were left to completely dry overnight. The films were then sealed between the coverslip and a glass microscope slide using UV curing epoxy. To protect the UV sensitive DPA molecules and CdSe surface, a small disk covered in aluminum foil was used to cover and protect the center of the film during the UV curing process, leaving only the edge of the coverslip exposed to the UV light (see SI for details). In order to characterize the films, profilometry experiments were performed on the blended film, the layered film, and a single layer of the layered morphology giving thicknesses of approximately 6 microns for each drop cast layer (Figure 5.10). These are summarized in Table 4.1.

The blended and layered films were then tested for upconversion using a 532 nm CW laser using a front face detection geometry. We note that without the 9ACA transmitter on the CdSe nanocrystals, no photon upconversion was observed. More than ten spots on each film gave strong upconversion signal and were investigated, with the upconversion signal varying based on spot location. The average upconversion signal in the center of the film was about the same, with large increases in upconversion signal being found at the edges of the film where both the film thickness was greatest and where UV curing epoxy touched each film. These best upconverting edge spots were included in our analysis, but due to increased thickness and variability of absorption at these edges are not the focus of this study. Due to the variation in the upconversion signal throughout both films, it was difficult to use an integrating sphere to locate certain spots. Thus we measured the relative quantum yield by employing an R6G thin film as the fluorescent standard in the same PVK polymer host. The fluorescence QY of this R6G standard was measured in an integrating sphere to be 24% (as described in the SI). The reference film was then placed in the same

front face detection geometry and used to quantify the upconversion signal for all films. In order to verify the accuracy of this approach, the best blended upconverting thin film was also measured in both the integrating sphere and front face geometry. The middle gave a similar upconversion QY close to 1.5% in both relative and absolute upconversion QY measurements. The overall upconversion efficiencies for the highest performing and average upconverting spot on the blended and layered thin films are summarized in Table 4.1. In general, the average photon upconversion QY is about 1.5% for the blended and 1.0% for the layered film using a 532nm CW laser with power densities exceeding 10 W/cm^2 (Figure 5.12) At the edges, the upconversion signals were approximately 4 and 2-fold higher for the blended and layered film, respectively. In solution, these CdSe/9ACA NCs in 3mM toluene have photon upconversion QY of 10.0%.[6]

Table 4.1 Summary of blended and layered thin film properties, including profilometry thickness measurements, upconversion quantum yield for the best spot and average center spot. ϕ_{TET2} values were calculated using $\phi_{TET1} = 0.813$ and $\phi_{DPA} = 0.659$ for both films

	Blended Film	*Layered Film*
Thickness (μm)	6.21 ± 0.42	11.33 ± 1.16
UCQYavg	0.015 ± 0.002	0.010 ± 0.002
UCQYbest	546	56.8
DPA/CdSe mol ratio	0.551	0.376
$\boldsymbol{\Phi_{TET2}}$***avg***	0.102	0.099
$\boldsymbol{\Phi_{TET2}}$***best***	5.1	6.5
$\boldsymbol{\Phi_{TTA}}$	6.21 ± 0.42	11.33 ± 1.16
DPA triplet lifetime (μs)	0.015 ± 0.002	0.010 ± 0.002

From the thickness measurements of these films, we calculated the concentration of CdSe/9-ACA and DPA in each film using Beer's law, treating each component as a solute dissolved in a solution of PVK and assuming the extinction coefficients in solution for DPA and CdSe did not change drastically from toluene to PVK. From this treatment,

we calculated the relative concentrations of DPA/CdSe to be an order of magnitude larger in the more efficient blended film compared to the layered film (Table 4.1 and Table 5.6). To further explore the efficiency of these films, we made several control films to study the intermediate processes that occur during upconversion. The first control film was and PVK film containing 20 wt% DPA only, allowing for better characterization of the DPA in the matrix. Then two CdSe in PVK films were made, the first with CdSe capped with its native oleic acid (OA) ligands, and the second containing CdSe capped with 9-ACA transmitter ligands without any DPA. The transient absorption spectra for the blended, layered, CdSe/OA and CdSe/9ACA films can be seen in Figure 5.14 and Figure 5.15.

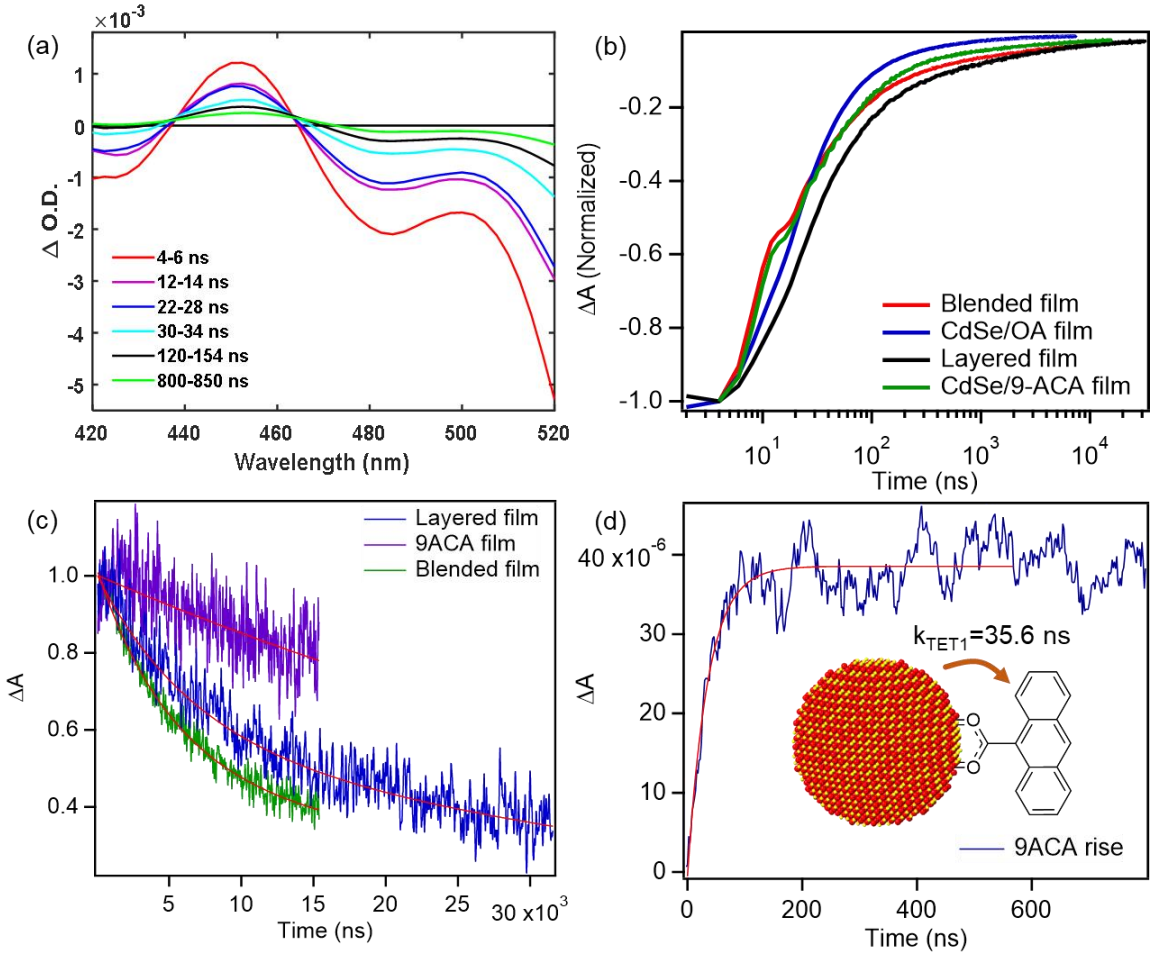

Figure 4.2 (a) Transient absorption (TA) spectra for the blended film. (b) Normalized ground state bleach kinetics measured at 510 nm. (c) Normalized TA kinetics at 440 nm peak of triplet excited state for CdSe/9-ACA only, blended, and layered films. (d) Growth of the triplet state in the CdSe/9-ACA only thin film corresponding to the rate of triplet energy transfer from the CdSe NC to the bound 9-ACA ligand. Transient absorption kinetics were analyzed at 440 nm after subtraction of early 0-20ns CdSe only component.

Equation 4.1 below relates the overall photon upconversion efficiency to the efficiencies of intermediate processes that occur:

$$\phi_{UC} = \phi_{TET1}\phi_{TET2}\frac{\phi_{TTA}}{2}\phi_{DPA} \tag{4.1}$$

where ϕ_{TET1} is the efficiency of TET from CdSe to bound 9-ACA ligand, ϕ_{TET2} is the efficiency of TET from the 9ACA transmitter to DPA, ϕ_{DPA} is the fluorescence quantum

yield of DPA. ϕ_{TTA} is the efficiency of TTA and is divided by two in order since the convention is that the maximum $\phi_{TTA} = 1$, because TTA is a two-to-one photon conversion process. Thus, we adopt the convention where the maximum $\phi_{UC} = 0.5$ here.

To quantify the DPA fluorescence QY, we used the integrating sphere to characterize this 20 wt % DPA in PVK thin film prepared and sealed in an air free nitrogen glovebox, excited at 365 nm. The resulting ϕ_{DPA} was 66 %, which is lower than the $\phi_{DPA} = 90\%$ in toluene. This decrease in fluorescence efficiency could be due to aggregation of DPA in the polymer matrix. Evidence of this aggregation is also observed in the red shifted photoluminescence of DPA in the blended and layered thin films compared to DPA in solution as shown in Figure 5.16.

We next sought to understand **TTA** efficiency by comparing the triplet lifetime in the CdSe/9-ACA thin film, which would not have any **TTA,** to the triplet kinetics in the blended and layered film morphologies. The blended and layered films both contain significant amounts of DPA, which is not present in the CdSe/9-ACA film. The trajectories of the anthracene triplet excitons in all three films were isolated after subtraction of the CdSe component dominant at early times in the TA measurements (see Figure 5.17). As can be seen in Figure 4.2c, the anthracene triplet decays faster when DPA is present in the films. Since DPA is more rigid, the non-radiative decay rate, k_{nr}, should be lower than the corresponding rate for 9-ACA, meaning that the DPA triplet lifetime should be as long as the less rigid 9-ACA, if the DPA molecules were electronically isolated. Depletion of DPA triplet excited states may through triplet-triplet annihilation, triplet-charge annihilation,[63] phosphorescence or triplet excimer formation.

In order to extract the DPA triplet lifetimes, the blended, layered, and CdSe/9-ACA in PVK films were globally fit at 440 nm, which is the peak maxima corresponding to the excited state absorption of anthracene. This fit assumes that 9ACA and isolated DPA decay with the same lifetime, and the aforementioned process quench the DPA triplet state. From these global fits, the 9-ACA/ isolated DPA lifetime decreased from 61.4 μs to 5.2 μs and 6.5 μs in the blended and layered films, respectively (Figure 4.2c). Assuming that triplet-triplet annihilation is dominant decay process for DPA, and statistically 1/9 of these collisions result in bright singlet states,[64] therefore given by equation (4.2)

$$\phi_{TTA} = 1/9\left(1 - {}^{\tau}/_{\tau_0}\right) \tag{4.2}$$

where τ_0 is the lifetime of the 9-ACA on CdSe (61.4 μs), and τ is the triplet lifetime of DPA in the blended and layered films (5.1 μs and 6.5 μs respectively). From equation 2 we can see the **TTA** efficiencies for blended and layered morphologies are 10.2% and 9.9% respectively.

The efficiency of the first triplet energy transfer term depends on the rate of triplet energy transfer from the CdSe NC to the bound 9-ACA ligand. We have shown that with smaller size CdSe NCs, the driving force for triplet energy transfer from the CdSe to the bound 9-ACA ligand is larger, minimizing back transfer from the ligand to the NCs.[6, 40] This allows for the assumption of unidirectional **TET1** from NC to transmitter.[47] From the isolated 9-ACA triplet kinetics obtained from the TA spectra of the CdSe/9ACA in PVK sample, we were able to monoexponentially fit a triplet rise of 35.6 ns after subtracting the CdSe component from early times (0-20 ns). The results are shown in Figure 4.2d (and

Figure 5.18). In toluene, the corresponding **TET1** time constant is 112.5 ns.[6] This makes sense given that mid-size green absorbing CdSe NCs are used in this work.[6, 40] From biexponential fits to the CdSe/OA in PVK sample at the same wavelength, we calculated the amplitude averaged lifetime of CdSe/OA according to equation 3, $\tau_{CdSe-OA} = 154.2$ ns (see Table 5.8). From these time constants where τ_{TET1}=35.6 ns, we can then calculate the efficiency of **TET1** using equation 4, where $\phi_{TET1} = 0.813$.

Equation (4.3). Amplitude averaged lifetime

$$\bar{\tau} = \frac{\sum_i A_i * \tau_i}{\sum_i A_i} \tag{4.3}$$

Equation (4.4). ϕ_{TET1}, Efficiency of triplet energy transfer from CdSe NC to 9-ACA transmitter ligand

$$\phi_{TET1} = \frac{1/\tau_{TET1}}{1/\tau_{TET1} + 1/\tau_{CdSe-OA}} \tag{4.4}$$

We can calculate ϕ_{TET2} from equation (4.1 after measuring $\phi_{UC}, \phi_{TET1}, \phi_{TTA}$and ϕ_{DPA}. Solving for ϕ_{TET2}, the efficiency for triplet energy transfer from the 9-ACA to DPA ranges from 6.1% on average to 24.5% at best (on the edges) for the blended film. $\phi_{TET2}$is lower in the layered film ~4.2 - 10.0%. The average values for ϕ_{TET2} about the same for both films (Table 4.1). We note that back transfer in the blended film is expected to be worse than in the layered morphology due to the closer proximity of CdSe to DPA. Lin et al reported that using a layered morphology, back transfer in their molecular films decreased to 8% from 60.3% compared to a blended structure.[63] One possible reason for

this disparity may be the inhomogeneous distribution of CdSe/9-ACA in the final films. The current drop casting technique is not sufficient to evenly distribute CdSe/9-ACA throughout the final film. While the CdSe/9-ACA does not appear to be visually excluded from the center of the films when examined by eye (Figure 4.3a inset), nanocrystals are concentrated in the edges of the film that dry first. PL mapping experiments confirm that the CdSe is concentrated at the edges of the final film and that clusters of emissive CdSe NCs are non-uniformly distributed in select spots in the middle of the blended film (Figure 4.3b). These spots appear to correspond to the areas of highest upconversion, and therefore higher ϕ_{TET2}. The DPA within the films is more uniformly distributed, as PL mapping exciting with 405 nm light shows uniform DPA emission throughout the center of the film (Figure 4.3c).

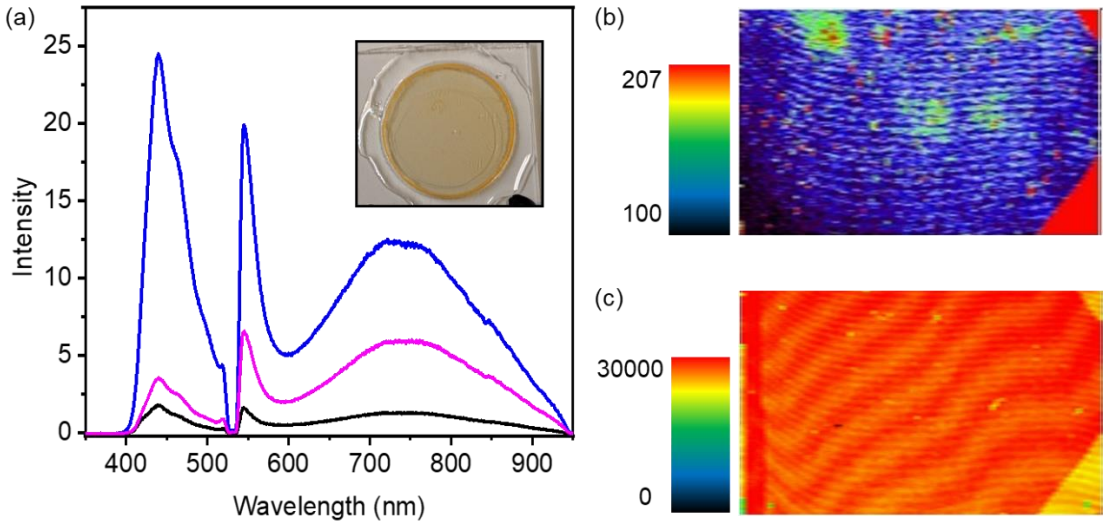

Figure 4.3 Upconversion spectra of blended film excited with 532 nm CW laser (a), photo of blended film morphology sealed thin film inset. Photoluminescence mapping data of blended film exciting the CdSe NCs at 532 nm (b) and exciting DPA at 405 nm (c).

In order to address these deficiencies introduced by drop-casting, spin coating techniques can be used to increase uniformity through the films, as well as better control over the final thickness. Clearly, increasing ϕ_{TET2} provides the greatest opportunity for increasing the upconversion QY for these films. In solution, **TET2** is usually diffusion limited when DPA is available in millimolar concentrations at its solubility limit. In the final PVK thin films, the DPA concentration is at least two orders of magnitude higher at 0.5 M (Table 5.6), and these high concentrations of DPA should favor TET from photosensitizer to annihilator. The long oleic acid chains on CdSe quite possibly form a tunneling barrier to TET2. Finally, ϕ_{UC} can also be improved by increasing the photoluminescence QY of the thin film by including singlet traps as dopants. This strategy by Ogawa et al will reduce FRET-based back transfer from DPA to the nanocrystal.[65]

Here we have shown initial success transforming our nanocrystal sensitized TTA based upconversion system from volatile organic solvents to a thin film with upconversion

quantum yields on par with the best organic TTA-based thin films. The use of PVK allows a high concentration of DPA to be incorporated while eschewing phase separation of the photosensitizer and annihilator. The key bottleneck in these thin films is the second step of triplet energy transfer, which may be addressed with transmitter ligands that facilitate triplet energy transfer via a hopping mechanism,[66] or with shorter solubilizing ligands on the NCs.[33] Our current upconversion efficiencies of 0.015 out of a maximum of 0.5 can be significantly improved by increasing the DPA fluorescence QY and modifying our fabrication techniques to produce more uniform thin films. Better control over the distribution of CdSe/9-ACA within the films will enhance TET2 and therefore the overall upconversion efficiencies of these films. With future improvements and the viability of environmentally friendly, non-toxic InP or silicon based light absorbers,[21] these films may yet find use in practical solar or biomedical applications.

Chapter 5 Supporting Information

5.1 Chemicals

Cadmium oxide (CdO, 99.99%), oleic acid (OA, tech. grade, 90%), and 1-octadecene (ODE, 90%) were purchased from Aldrich. Selenium (Se, 99.9%) was purchased from Strem Chemicals, and toluene was purchased from Fisher and dried and degassed using JC Meyer's solvent purification system.

5.2 Instrumentation

Linear absorption spectra were recorded on a Cary 5000 UV-Vis absorption spectrophotometer. Photoluminescence (PL) of CdSe nanocrystals (NCs) were recorded on Spex Fluorolog Tau-3 fluorescence spectrophotometer. Photoluminescence quantum yield was obtained with the standard of rhodamine 6G in ethanol.

5.3 Synthesis of CdSe NCs

2.3 nm diameter zb-CdSe NCs were synthesized following the modified method of Zhang et al:[67] 230 mg CdO, 1.6 mL oleic acid and 14.25 mL 1-octadecene were added into a 50 mL 3-necked round bottom flask and heated at 120 ^{o}C for 1 hour under vacuum. The flask was then filled with argon. The flask was then heated to 270 ^{o}C and once the solution turned clear, the temperature was set between 270 ^{o}C and 290 ^{o}C depending on the desired final size of the nanocrystal. Once the injection temperature was reached, 2.5 mL of a 0.4 M suspension of Se powder in ODE was injected and the reaction flask was cooled to room temperature with compressed air for the smallest particles and allowed to cool naturally for large sizes. Nanocrystals were washed two times by

precipitation/redispersion with ethanol/hexane and washed a final time in hexane/acetone. Cleaned particles were re-dispersed in toluene and stored in the dark.

5.4 Preparation of samples for transient absorption and upconversion measurements

Ligand exchange reactions are performed by mixing CdSe NCs with 9-anthracenecarboxylic acid (9-ACA) at different concentrations in THF, as described in Table 5.1, and then stirred overnight. Total volume of ligand exchange solution is 190 µL. After ligand exchange, 1 mL acetone was added as a bad solvent to precipitate out the nanocrystals, and the CdSe/9-ACA complex was precipitated by centrifuging for 10 min at 7830 rpm. The clear supernatant containing excess 9-ACA ligand was discarded.

For upconversion measurements, the CdSe/9-ACA pellet was re-dispersed in 3 mM DPA/toluene solution and then transferred to a 1 cm path length Starna cuvette. For transient absorption measurements, the pellet was re-dispersed in toluene to make a solution with optical density = 0.3 at the excitation wavelength in a 1 mm path length airtight cuvette. All samples were prepared and sealed in a nitrogen glovebox.

Table 5.1 Extinction coefficients for CdSe samples and 9-ACA ligand exchange conditions

	Wavelength (nm)	*$\varepsilon(M^{-1} \cdot cm^{-1})$*	*[CdSe] in ligand exchange (µM)*	*[9-ACA] in ligand exchange (mM)*
CdSe A	505	53886	105	400
CdSe B	511	57566	105	6.28
CdSe C	523	66666	105	11.51
CdSe D	552	105132	105	2.09
CdSe E	591	250596	105	2.09
CdSe F	612	445819	105	3.66
CdSe G	615	486396	105	1.09
9-ACA	389	7800	-	-

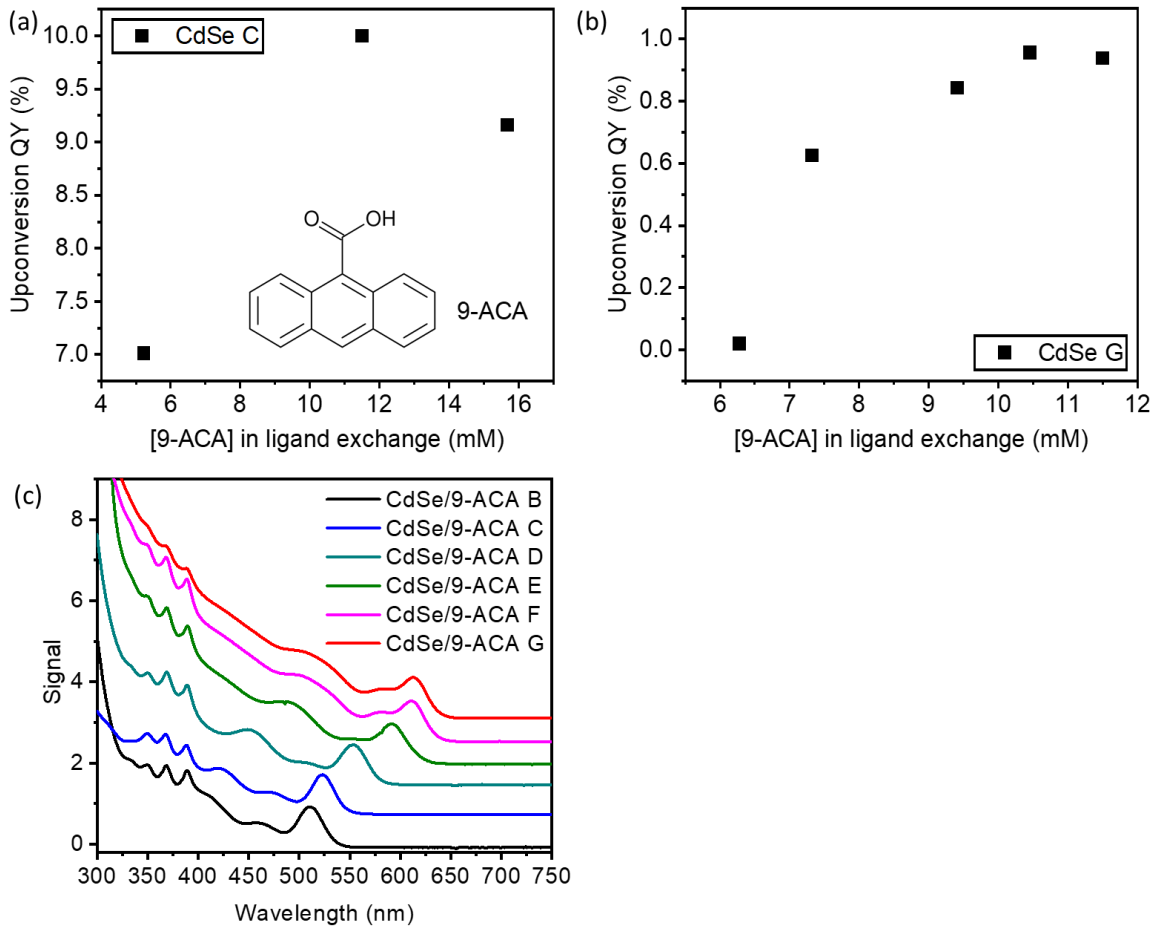

Figure 5.1 Optimization of upconversion quantum yields against the concentration of ligands in ligand exchange solution for 9-ACA for (a) CdSe C and (b) CdSe G. (c) Absorbance spectra of CdSe NC ligand exchanged with 9-ACA.

5.5 Upconversion and photoluminescence measurements

Upconversion fluorescence spectra were recorded from the right angle to the excitation with an Ocean Optics Inc. Maya Pro 2000 spectrometer. The 532 nm excitation produced by Ti:Sapphire laser (Coherent) focused to a spot with diameter of 120.9 μm resulting in flux of 12.7 W/cm^2. In front of the detector, a 532 nm, 25 nm bandwidth notch filter (part number NF01-532U-25) has been used to block residual excitation light. The upconverted signal was collected in perpendicular geometries and focused into a PAF-SMA-11-A (Thor Labs) fiberport through an Ocean Optics QP400-2-SR fiber connected to the Maya Pro 2000 spectrometer system. All samples were prepared in air tight Starna cuvettes with screw tops in a nitrogen glove box. The upconversion quantum yields were calculated using rhodamine 6G as standard with the 532 nm laser.

5.6 Upconversion quantum yield calculations

The photon upconversion (UC) QY, Φ_{UC} is defined as:

$$\Phi_{UC} = 2 \times \Phi_{ref} \times \frac{(photons\ absorbed\ by\ reference)}{(photons\ absorbed\ by\ UC\ sample)} \times \frac{PL\ signal(UC\ sample)}{PL\ signal(reference)} \tag{5.1}$$

where Φ_{ref} is the photoluminescence QY of the rhodamine 6G reference, which is 95% in ethanol. The equation can be further broken down to better represent how these measurements are taken by equation (5.2).

$$\Phi_{UC} = 2 \times \Phi_{R6G} \times \frac{n_{DPA}^2}{n_{R6G}^2} \times \frac{[Area]_{DPA}}{[Area]_{R6G}} \times \frac{1 - 10^{-A_{R6G}}}{1 - 10^{-A_{sample}}} \tag{5.2}$$

Where the n_{DPA} and n_{R6G} represent the refractive indices of the solvents in the sample and reference cuvettes, which are toluene and ethanol, respectively. The $[Area]_{DPA}$ and $[Area]_{R6G}$ are the integrated areas of the fluorescence peaks of the DPA signal from the upconversion sample and the R6G signal from the reference sample. The absorbance of the upconversion and R6G samples at the wavelength of excitation is represented by A_{sample} and A_{R6G}.

5.7 Upconversion spectra of CdSe/9-ACA and CdSe/2-ACA with octylamine

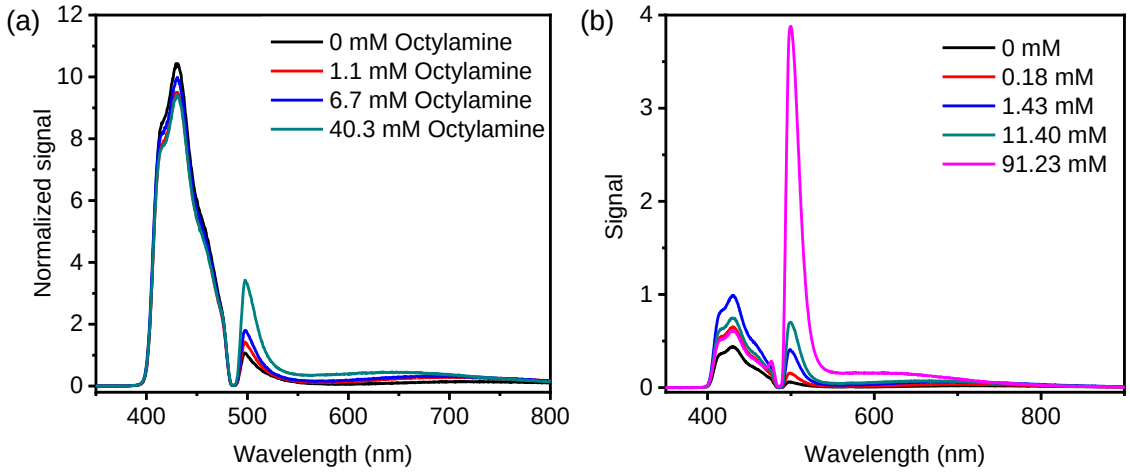

Figure 5.2 Photoluminescence spectra of photon upconversion with CdSe NC's functionalized with (a) **9-ACA** and (b) **2-ACA** bound on the surface in increasing concentrations of octylamine. Samples are dissolved in toluene and excited with 488 nm laser. All signals normalized by absorption at 488 nm.

5.8 Photoluminescence and upconversion spectra of CdSe/2-ACA with propylamine

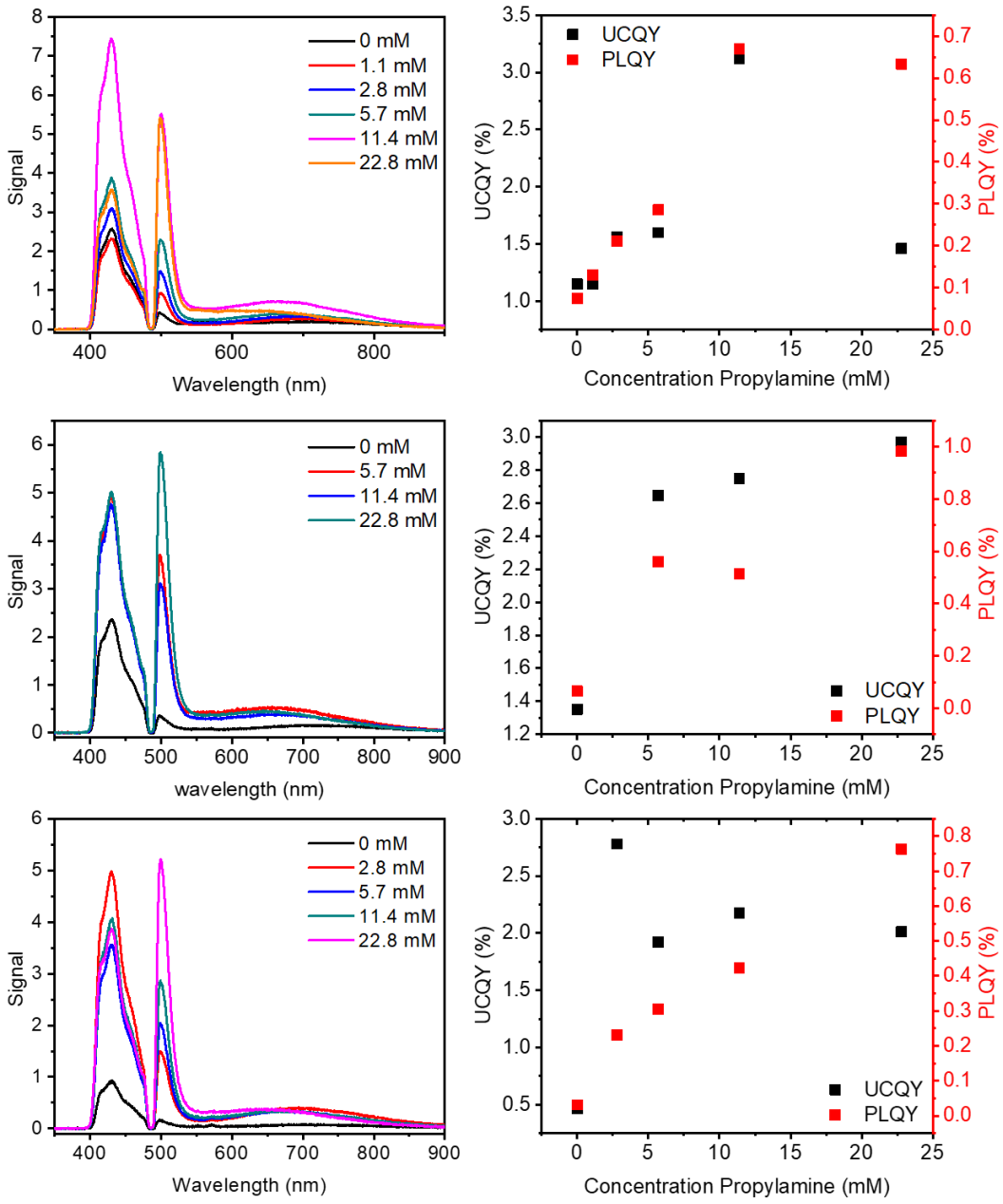

Figure 5.3 Photoluminescence (PL) spectra of photon upconversion (UC) with CdSe NC light absorbers functionalized with 2-ACA bound on the surface in increasing concentrations of propylamine. Samples are dissolved in toluene and excited with 488 nm laser. All signals normalized by absorption at 488 nm. All signals normalized by absorption at 488 nm. The photon upconversion and photoluminescence quantum yield vs concentration of propylamine is plotted on the right.

5.9 Measuring Transient Absorption Data

Nanosecond transient absorption measurements were performed using the enVISion spectrometer from Magnitude Instruments using 532 nm excitation pulses, with repetition rate varying from 1kHz to 10kHz, depending on the time window. The excitation energy density was 87 $\mu J/cm^2$ for a 10 kHz repetition rate.

Ultrafast transient absorption experiments were performed using the Ti:Sapphire chirped pulse amplified system SpitfireACE Spectra Physics, Newport Corp, 6 mJ @ 800 nm, 100 fs, 1 kHz) and Transient Absorption Spectrometer (TAS, Newport Corp.). The amplifier system is pumped using an Empower® Q-switched DPSS laser and seeded by a Mai Tai SP oscillator (90 fs, 80 MHz). The outcome of the regenerative amplifier was split in multiple paths. One beam was coupled to optical parametric amplifiers (OPA, Lightconversion TOPAS™) to generate a pump pulse at 540 nm (100 fs pulse duration). A small portion of the fundamental 800 nm beam was picked off and sent through a delay line and then focused into a 2 mm CaF2 crystal to generate a white light continuum. The generated supercontinuum is then focused onto the sample and overlapped with the pump beam. The transient spectra were detected with fiber-coupled CCD-based monochromator (Oriel, Newport).

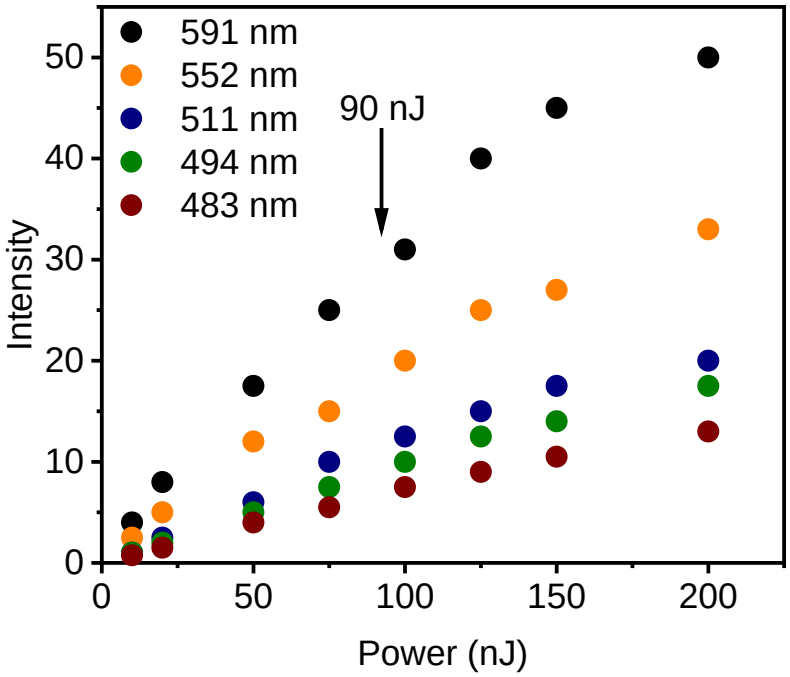

Figure 5.4 The emission intensity of five different CdSe NCs with decreasing absorption maxima at their individual wavelengths versus the excitation power obtained from the transient absorption setup. The laser power of 90 nJ was used to excite all samples to avoid exciton-exciton annihilation processes observed at higher powers. Samples were dissolved in toluene and excited with a corresponding wavelength pulsed laser at room temperature.

5.10 Transient absorption traces of CdSe and CdSe/2-ACA in varying concentrations of propylamine

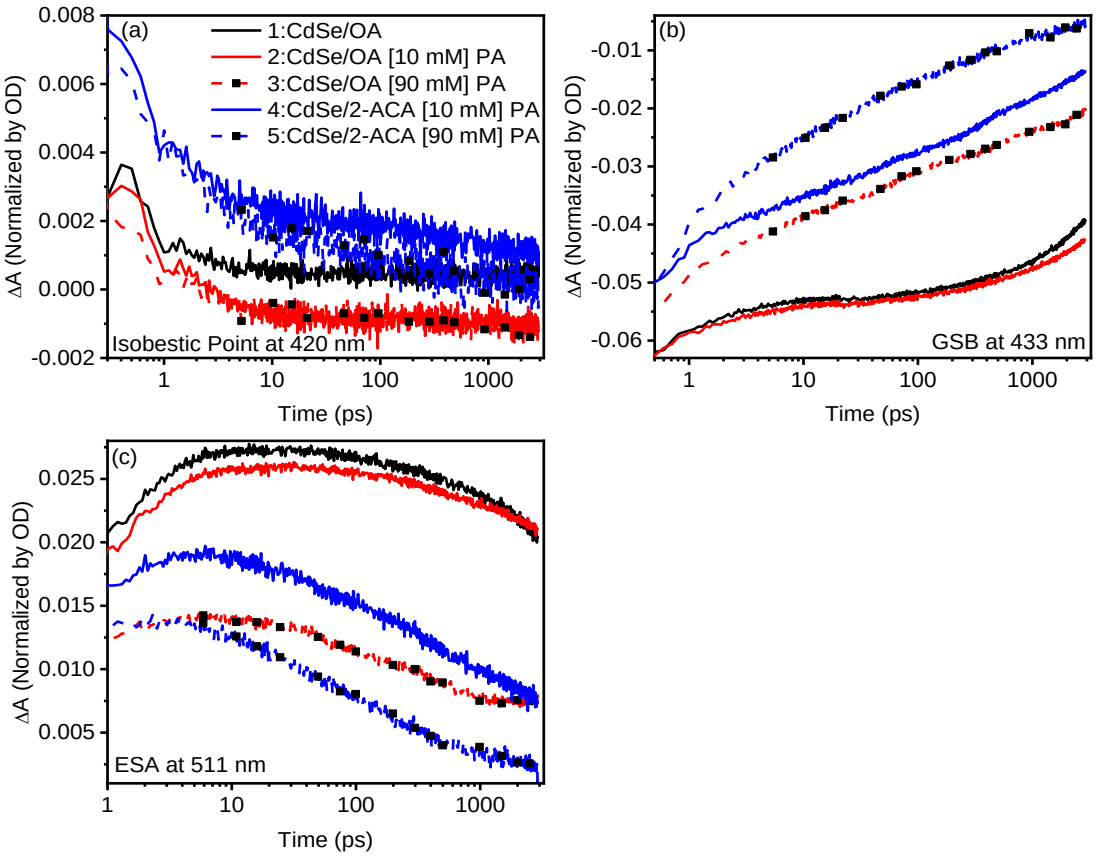

Figure 5.5 (a) Transient absorption (TA) traces at the isosbestic point (420 nm) showing contribution of TET to bound 2-ACA in samples 2 and 3, (b) Ground state recovery (GSB) at 433 nm, illustrating relative quenching of CdSe NC in the presence of both surface-bound 2-ACA and high concentrations of amine. (c) Excited state absorption (ESA) at 511 nm corresponding to the contribution of the trap state. All normalized by OD of nanocrystal at 487 nm for TA fits as opposed to Figure 2.4 (b)-(d) which is normalized by the time.

5.11 Global fitting graph and fitting parameters of transient absorption traces

Biexponential equation for NC only, two lifetimes, τ_0 and τ_1:

$$I(t) = A_0 * e^{-(t-t_0)/\tau_0} + A_1 * e^{-(t-t_0)/\tau_1} \quad (5.3)$$

Biexponential equation for NC with amine introducing additional decay components: τ_{N0}, τ_{N1}, τ_{N2}:

$$I(t) = A_0 * e^{\left[-\left(\left(\frac{1}{\tau_0}\right)+\left(\frac{1}{\tau_{N_0}}\right)\right)(t-t_0)\right]} + A_1 * e^{\left[-\left(\left(\frac{1}{\tau_1}\right)+\left(\frac{1}{\tau_{N_1}}\right)\right)(t-t_0)\right]} \quad (5.4)$$

Equation for CdSe NC with amine and 2-ACA transmitter ligand resulting in triplet energy transfer, τ_{TET}:

$$I(t) = A_0 * e^{\left[-\left(\left(\frac{1}{\tau_0}\right)+\left(\frac{1}{\tau_{N_0}}\right)\right)(t-t_0)\right]} + A_1 * e^{\left[-\left(\left(\frac{1}{\tau_1}\right)+\left(\frac{1}{\tau_{N_1}}\right)\right)(t-t_0)\right]} + A_2 * e^{\left(-\frac{t-t_0}{\tau_{TET}}\right)} \quad (5.5)$$

Table 5.2 Global fitting parameters of the kinetics at 433 nm from transient absorption for samples **1**–**5** using equations 1–3. All samples are corrected for time zero. A_0, A_1, and τ_0, τ_1 are the amplitudes and lifetimes of the decays of the NCs at 433 nm. A_2, τ_{N0}, τ_{N1}, τ_{N2}, and τ_{TET} are the amplitudes and lifetimes of the decays from the contribution of the amine and TET.

CdSe	**1: OA**	**2: OA**	**3: OA**	**4: 2-ACA+OA**	**5: 2-ACA+OA**
Propylamine [mM]	**0**	**10**	**90**	**10**	**90**
A_0	95.2±0.1%	93.8±0.1%	19.0±0.3%	26.2±0.3%	31.8±0.4%
A_1	4.8±0.1%	6.2±0.1%	18±0.3%	18.1±0.2%	35.2±0.4%
A_2	-	-	63±0.3%	55.7±0.3%	33.0±0.4%
τ_0 (ns)	11.09±0.08	11.09±0.08	11.12±0.04	11.09±0.08	11.12±0.04
τ_1 (ns)	0.177±0.009	0.177±0.010	0.179±0.006	0.177±0.009	0.180±0.006
τ_{N0} (ns)	-	-36.3±1.3	0.294±0.011	0.296±0.007	0.239±0.008
τ_{N1} (ns)	-	-1.55±0.89	0.0269±0.0010	0.0200±0.0056	0.0188±0.0046
τ_{N2a} (ns)	-	-	12.9±0.4	-	-
τ_{TET} (ns)	-	-	-	6.57±0.12	4.94±0.17
PLQY (%)	0.23	2.01	5.96	0.68	1.60
Trap QY (%)	0.80	4.33	2.35	0.71	0.68
Upconversion QY (%)	0	0	0	2.89	2.71
ΦTET (%)	-	-	-	1.18	1.57

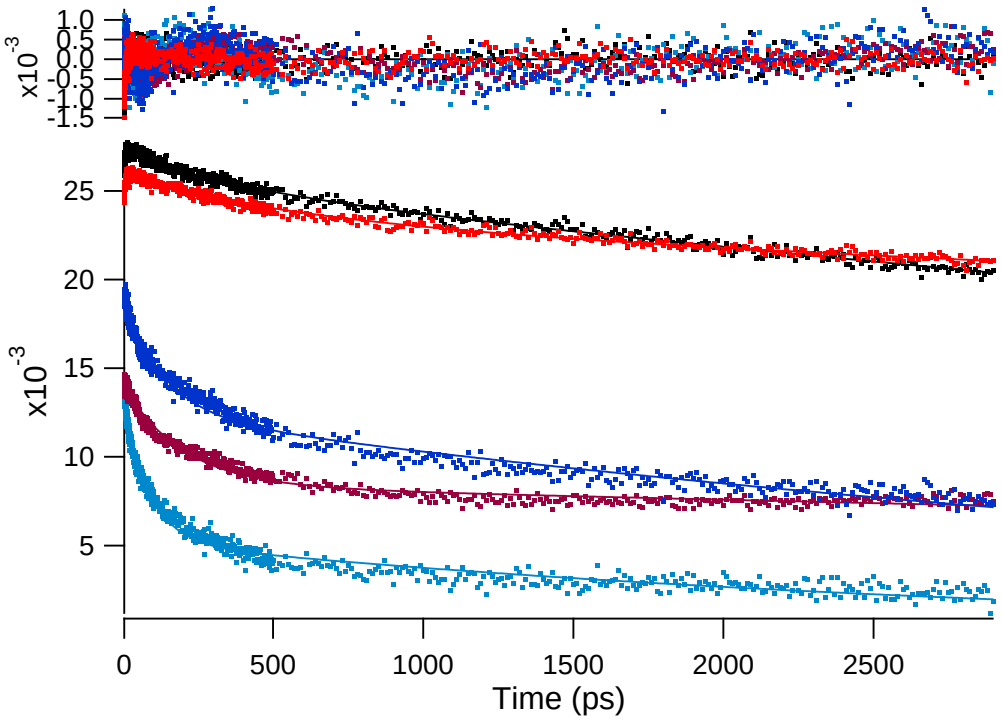

Figure 5.6 Analysis of the trap state from transient absorption data from samples **1**–**5.** The trajectories at 511 nm are graphed with sample **1** in black, sample **2** in red, sample **3** in wine, sample **4** in blue, and sample b in light blue. Global fitting results are shown, with residual traces plotted at the top.

Table 5.3 Global fitting parameters for the kinetics of the trap state, measured at 511 nm for samples **1**–**5** from transient absorption, as described in equations 1 and 2. All samples are corrected for time zero. A_0, A_1, and τ_0, τ_1 are the amplitudes and lifetimes of the decays of the NCs at 511 nm. τ_{N0}, τ_{N1}, and τ_{N2}, are the lifetimes of the decays from the contribution of the amine and TET.

CdSe	**1: OA**	**2: OA**	**3: OA**	**4: 2-ACA+OA**	**5: 2-ACA+OA**
Propylamine [mM]	**0**	**10**	**90**	**10**	**90**
A_0	93.5±0.5%	10.1±1.1%	60.2±0.5%	66.4±0.3%	40.6±0.4%
τ_0 (ns)	13.1±0.4	13.1±0.4	13.1±0.4	13.1±0.4	13.1±0.4
A_1	6.5±0.5%	89.9±1.2%	39.8±0.5%	33.6±0.3%	59.4±0.4%
τ_1 (ns)	0.365 ± 0.04	0.365 ± 0.04	0.365 ± 0.04	0.365 ± 0.04	0.365 ± 0.04
τ_{N0} (ns)	-	0.669 ± 0.09	-39.4 ± 8	8.73 ± 0.3	3.83 ± 0.1
τ_{N1} (ns)	-	-0.369 ± 0.04	0.432 ± 0.06	0.217 ± 0.02	0.112 ± 0.005

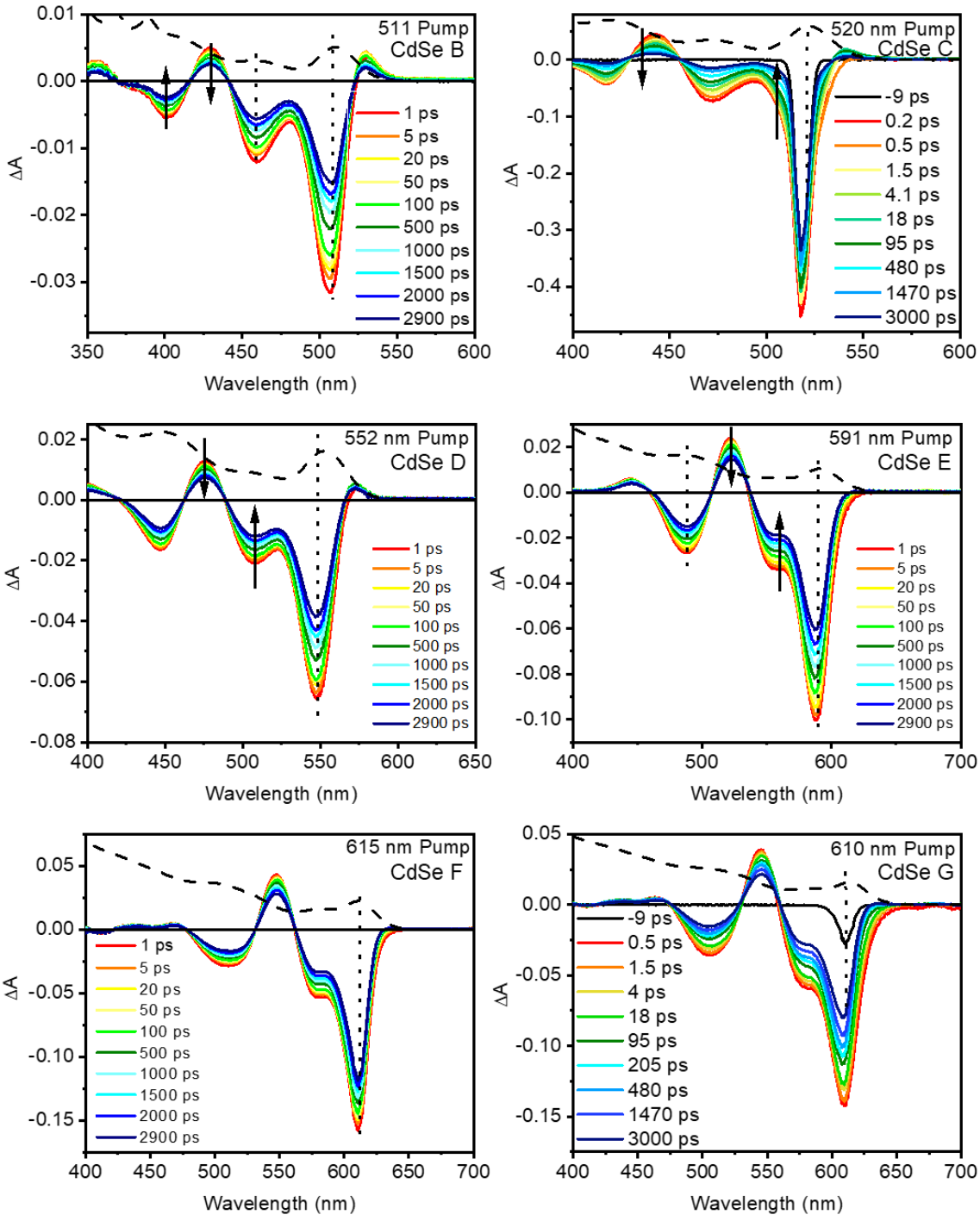

Figure 5.7 Ultrafast transient absorption spectra of six zb CdSe nanocrystals with diameters ranging from 2.5 – 5.3 nm and first excitons from 511 nm to 615 nm. Dotted lines show ground state bleach (GSB) and 430 nm corresponding to the growth of the 9-ACA triplet.

5.12 Global fitting equations and fitting parameters of transient absorption traces

Biexponential NC fitting with two lifetimes, τ_1 and τ_2:

$$I(t) = A_1 exp\left(-\frac{t-t_0}{\tau_1}\right) + A_2 exp\left(-\frac{t-t_0}{\tau_2}\right) \quad (5.6)$$

NC with transmitter ligand (9-ACA) introducing additional triplet decay component: τ_{TET}

$$I(t) = A_1 exp\left(-\frac{t-t_0}{\tau_1}\right) + A_2 exp\left(-\frac{t-t_0}{\tau_2}\right) + A_3 exp\left(-\frac{t-t_0}{\tau_{TET}}\right) \quad (5.7)$$

where t_0 is a time offset of 2 ps, A_3 is the maximum absorption of the 9-ACA triplet, τ_1 and τ_2 correspond to the intrinsic decay of the NC, and τ_{TET} is the net transfer of excited state energy between the nanocrystal and the 9-ACA ligand. Using a global fit allows the intensity of absorption to vary with wavelength, while linking the lifetime components.

Table 5.4 Fitting parameters for picosecond transient absorption data where global fits of the GSB of the CdSe nanocrystal and ESA of the NC and triplet energy transfer to the 9-ACA at 435 nm were performed.

	CdSe B GSB	CdSe B ESA	CdSe C GSB	CdSe C ESA	CdSe D GSB	CdSe D ESA
A_1	-2.01×10^{-3}	6.68×10^{-4}	-2.65×10^{-2}	4.81×10^{-3}	-1.88×10^{-3}	-1.14×10^{-3}
A_1 %*	18.1	20.8	33.7	8.3	20.0	10.0
τ_1 (ps)	126.7	126.7	34.7	34.7	10.5	10.5
A_2	-9.13×10^{-3}	2.29×10^{-3}	-5.22×10^{-2}	7.19×10^{-3}	-7.52×10^{-3}	-3.61×10^{-3}
A_2 %*	81.9	71.4	66.3	12.4	80.0	31.6
τ_2 (ps)	5.90×10^{3}	5.90×10^{3}	9.02×10^{2}	9.02×10^{2}	1.46×10^{3}	1.46×10^{3}
A_3	-	2.50×10^{-4}	-	4.59×10^{-2}	-	6.67×10^{-3}
A_3 %*	-	7.8	-	79.3	-	58.4
τ_{TET} (ps)	-	6.60×10^{1}	-	1.12×10^{5}	-	5.36×10^{6}

	CdSe E GSB	CdSe E ESA	CdSe F GSB	CdSe F ESA	CdSe G GSB	CdSe G ESA
A_1	-3.17×10^{-3}	4.24×10^{-4}	-3.13×10^{-3}	-3.30×10^{-5}	-1.43×10^{-2}	1.11×10^{-4}
A_1 %*	22.1	3.1	19.9	0.2	33.4	0.3
τ_1 (ps)	48.6	48.6	66.6	66.6	72.7	72.7
A_2	-1.12×10^{-2}	1.68×10^{-3}	-1.26×10^{-2}	2.06×10^{-3}	-2.85×10^{-2}	1.78×10^{-3}
A_2 %*	77.9	12.4	80.1	14.3	66.6	4.9
τ_2 (ps)	3.31×10^{3}	3.31×10^{3}	3.52×10^{3}	3.52×10^{3}	3.21×10^{3}	3.21×10^{3}
A_3	-	1.14×10^{-2}	-	1.23×10^{-2}	-	3.43×10^{-2}
A_3 %*	-	84.4	-	85.5	-	94.8
τ_{TET} (ps)	-	8.18×10^{6}	-	1.77×10^{7}	-	1.48×10^{7}

*Values for A_1, A_2, and A_3 normalized to 100%

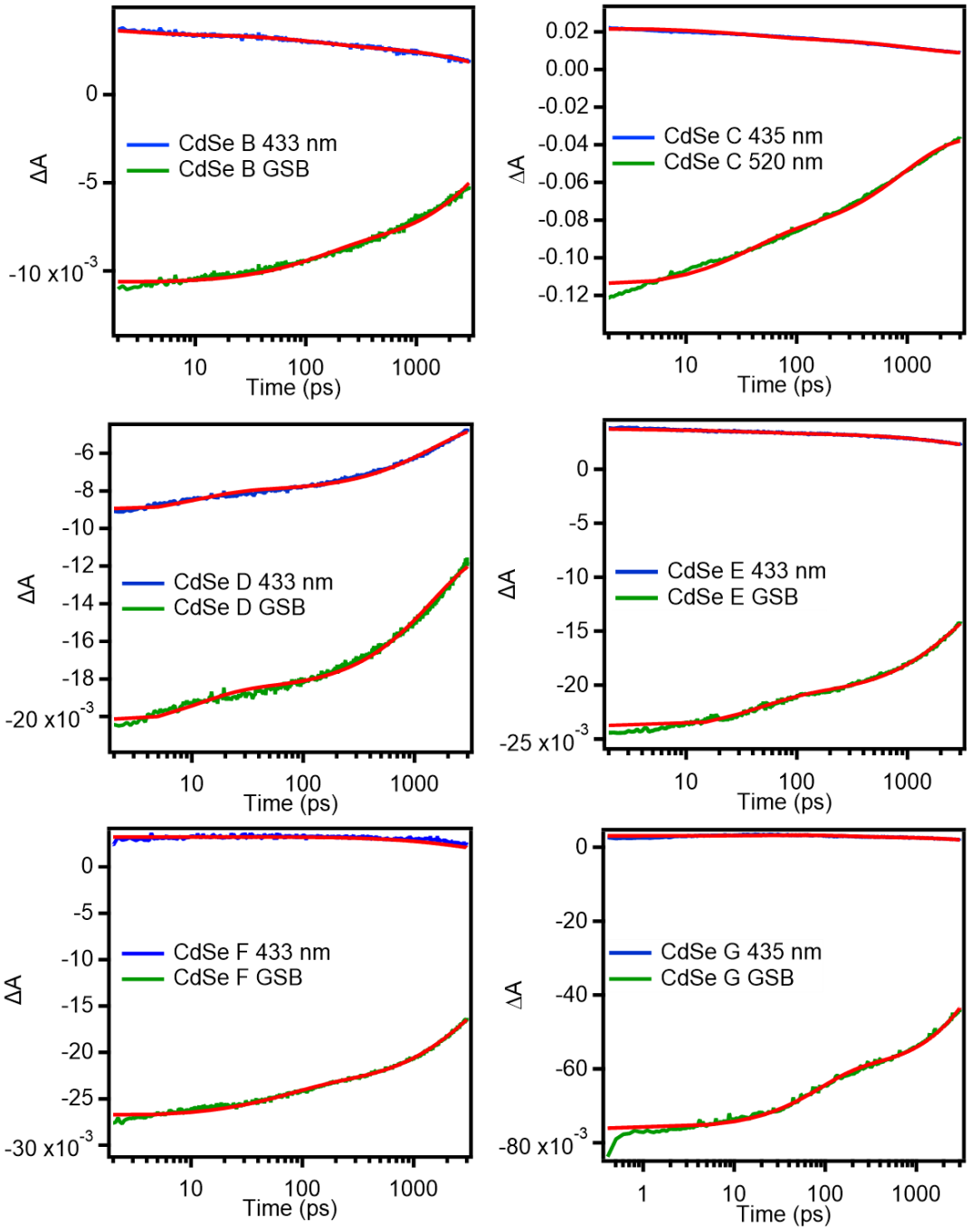

Figure 5.8 Global fitting results (red) for ultrafast transient absorption traces of six CdSe/9-ACA samples in toluene. The 433-435 nm traces show the 9-ACA triplet (blue), while the ground state bleach (GSB, green) of each CdSe nanocrystal was measured 30 nm blue of the excitation wavelength at the first excitonic peak of the NC.

5.13 Amplitude and intensity averaged lifetimes for CdSe G

Equation for amplitude weighted averaged lifetime

$$\bar{\tau} = \frac{\sum_i A_i * \tau_i}{\sum_i A_i} \tag{5.8}$$

Equation for intensity weighted averaged lifetime

$$\bar{\tau} = \frac{\sum_i A_i * \tau_i^2}{\sum_i A_i * \tau_i} \tag{5.9}$$

Table 5.5 Amplitude and intensity weighted lifetimes of CdSe-G NCs with and without 9-ACA, $\tau_{G\text{-}AN}$ and τ_G respectively, as monitored by the recovery of the CdSe NC ground state bleach at 605 nm, excited at 532nm, measured with ns-TA.

					Lifetime (ns)	
	A_1	τ_1 (ns)	A_2	τ_2 (ns)	Amplitude	Intensity
CdSe G-AN	-0.00476	6.3	-0.00175	34.6	13.9	25.3
CdSe G	-0.0125	4.9	-0.00307	27.3	9.3	17.9

5.14 Ligand loading and fabrication of thin film samples for upconversion, transient absorption, and upconversion measurements

Ligand exchange reaction was performed by mixing CdSe NCs with 9-ACA at different concentrations in THF and then stirring overnight. Total volume of ligand exchange solution is 190 µL. After ligand exchange, 1 mL acetone was added as a bad solvent to precipitate out nanocrystals, and the CdSe/9-ACA complex was precipitated by centrifuging for at least 10 min at 7830 rpm. The clear supernatant containing excess 9-ACA ligand was discarded.

To test for optimal loading, an upconversion measurement was performing by redispersing the CdSe/9-ACA pellet in 2 mL 3 mM DPA/toluene solution and then

transferred to a 1 cm path length Starna cuvette. The ligand loading which produced the highest upconversion QY was then used throughout the rest of the thin film fabrication experiments.

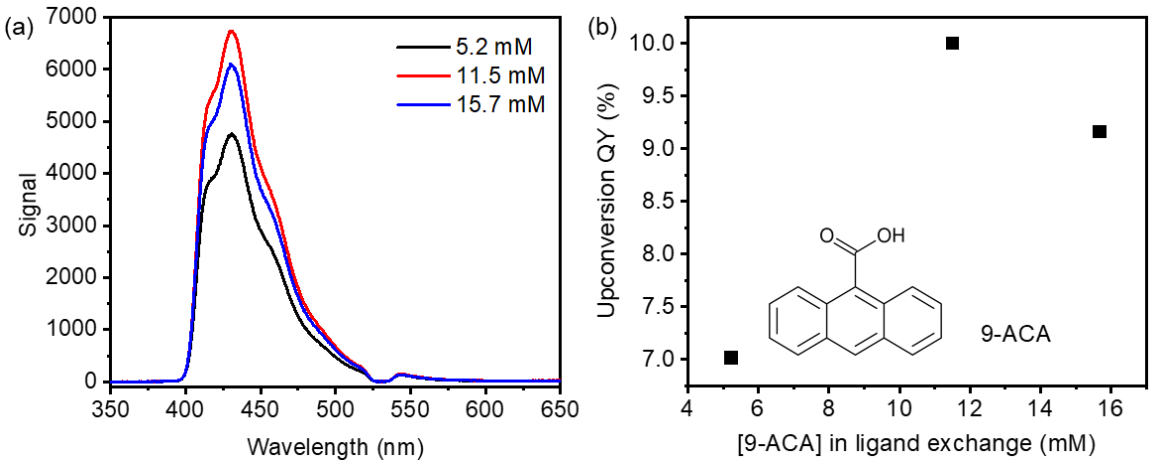

Figure 5.9 Ligand loading optimization for CdSe nanocrystals. (a) Upconversion signal for three different ligand loading concentrations. (b) Upconversion QY vs concentration of 9-ACA ligand in ligand exchange solution.

Thin film samples were drop casted from a 20 wt% DPA in PVK solution in 1,2-dichlorobenzene. 0.4 mL of each solution was dropped onto a uniform cleaned glass coverslip and allowed to completely dry overnight. Dry samples were sealed onto a clean glass microscope slide using UV curing epoxy.

R6G reference thin film was fabricated by adding R6G to a sample of 8 mg PVK dissolved in 1 mL *o*-DCB in a nitrogen glovebox. 400 µL of the final solution was drop casted onto a 25 mm glass coverslip. R6G concentration was designed so that the resulting thin film absorbance was within 0.05 of the absorption of the upconverting thin films at 532 nm.

All samples were prepared in a nitrogen glovebox.

5.15 Profilometry experiments

Profilometry experiments were performed using a Dektak8, Bruker profilometer using a standard scan and 5 micrometer radius stylus. Twenty second scans were performed for 17-22 nm depending on the sample with a force of 5 mg and a measurement range of 655 kAngstrom.

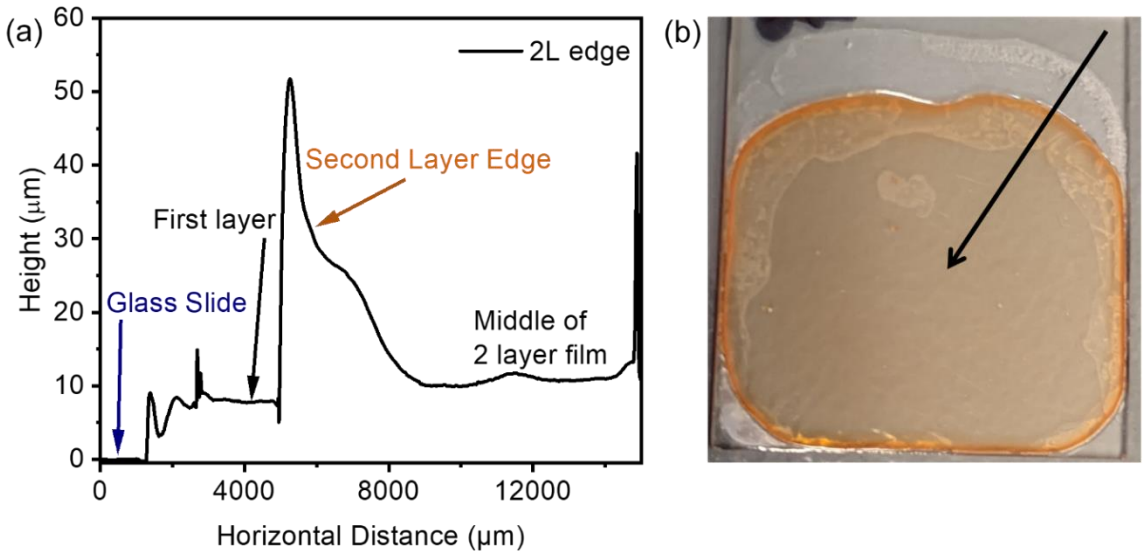

Figure 5.10 Profilometry of layered thin film morphology showing glass slide, bubbles formed on edge of first layer, large edge of the second CdSe containing layer and middle of the completed layered film.

5.16 Concentration of DPA and CdSe in blended and layered film morphologies

Concentration of DPA and CDSe/9-ACA in PVK was determined by Beer's law.

$$A = \varepsilon * C * t \tag{5.10}$$

Where A is the absorption of the film, ε is the molar absorptivity, and t is the thickness of the film in cm.

Table 5.6 Summary of thickness, molar absorptivity, and concentration of DPA and CdSe/9-ACA in both layered and blended film morphologies. The molar absorptivity of DPA at 372.5 nm is 1.40 x10^4 cm-1/M and molar absorptivity of CdSe at 523 nm is 6.67 x10^4 cm^{-1}/M.

	Thickness (cm)	[DPA]	[CdSe]	**DPA/CdSe**
Layered	7.57×10^{-4}	2.30×10^{-1}	2.05×10^{-3}	**56.8**
Blended	5.84×10^{-4}	5.74×10^{-1}	1.05×10^{-3}	**546.1**

5.17 Upconversion quantum yield measurements for thin films

The photon upconversion (UC) QY, Φ_{UC} is defined as:

$$\Phi_{UC} = 2 \times \Phi_{ref} \times \frac{(photons\ absorbed\ by\ reference)}{(photons\ absorbed\ by\ UC\ sample)} \times \frac{PL\ signal(UC\ sample)}{PL\ signal(reference)} \tag{5.11}$$

where Φ_{ref} is the photoluminescence QY of the rhodamine 6G reference, which is 95% in ethanol.

The quantum yield is defined as the ratio of emitted photons to absorbed photons, meaning that the theoretical maximum quantum efficiency of upconversion materials is defined as 50%, because the absorption of a minimum of two photons is required to generate one upconverted photon. All upconversion measurements were performed with an incident laser power in the linear regime for photon upconversion, meaning that triplets could be formed faster than they were depleted by TTA or other decay processes.

The PL quantum yield of the reference R6G in PVK thin film was measured using an absolute quantum yield measurement using a Labsphere RT-060 integrating sphere, exciting with a CW 532 89.5 μm beam radius laser, and detecting with a Maya Pro 2000 spectrometer detector.[68]

5.18 Beam radius and power dependence measurements

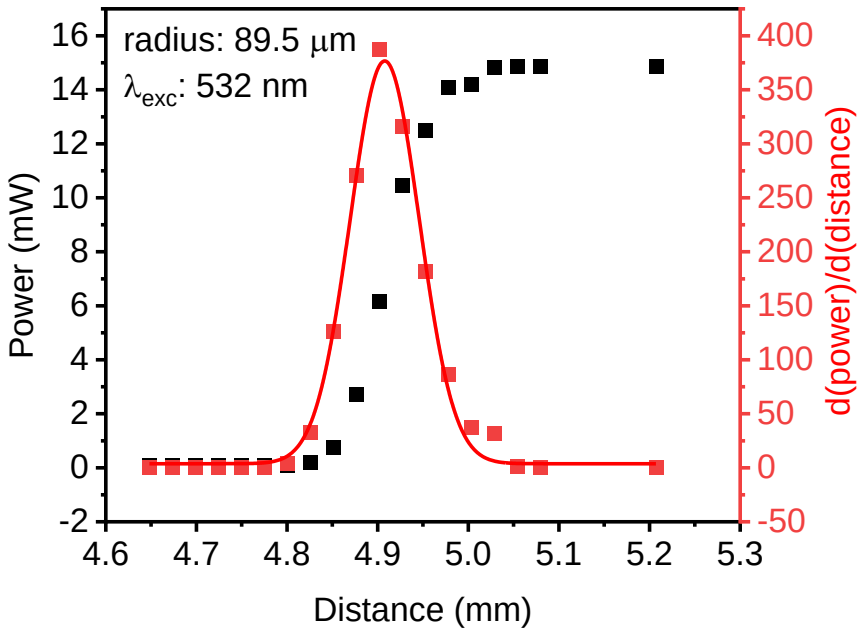

Figure 5.11 Laser intensity (black squares) decreases as the razor blade blocks the excitation source. The first derivative of the laser intensity (red squares) with respect to distance, d(power)/d(distance). The radius of the excitation light is obtained with a Gaussian fit (red curve).

To verify that the measurements were performed in the linear regime without multiphoton annihilation occurring in the NCs the power dependence was measured. Figure 5.12 shows that the upconversion signal versus excitation power shows a linear trend in the whole excitation interval indicating that no multi-photon annihilation occurs at the excitation power used in our experiments.

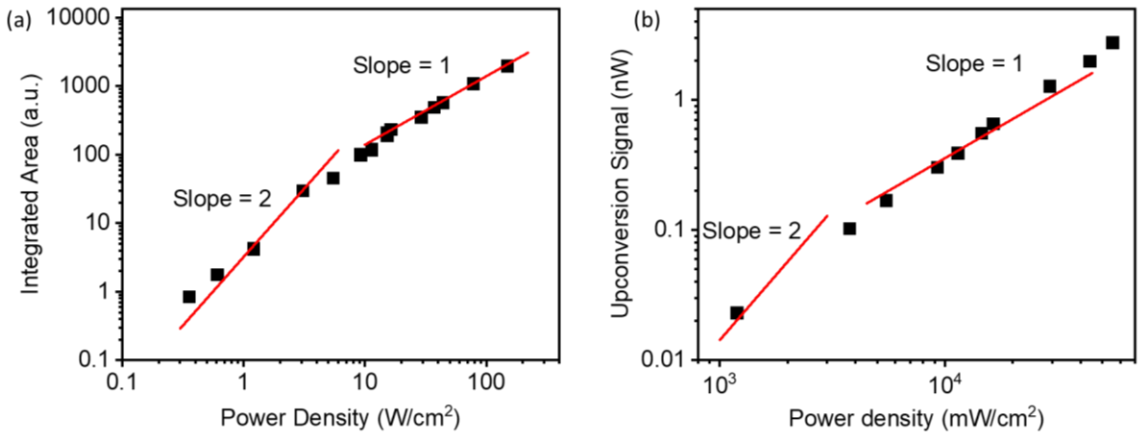

Figure 5.12 Power dependence on best upconverting spot (a) and alternate spot (b) of blended thin film morphology. Thin film excited with 532 nm CW laser, and signal monitored by front face detection and integrating the upconversion signal from 380-513 nm.

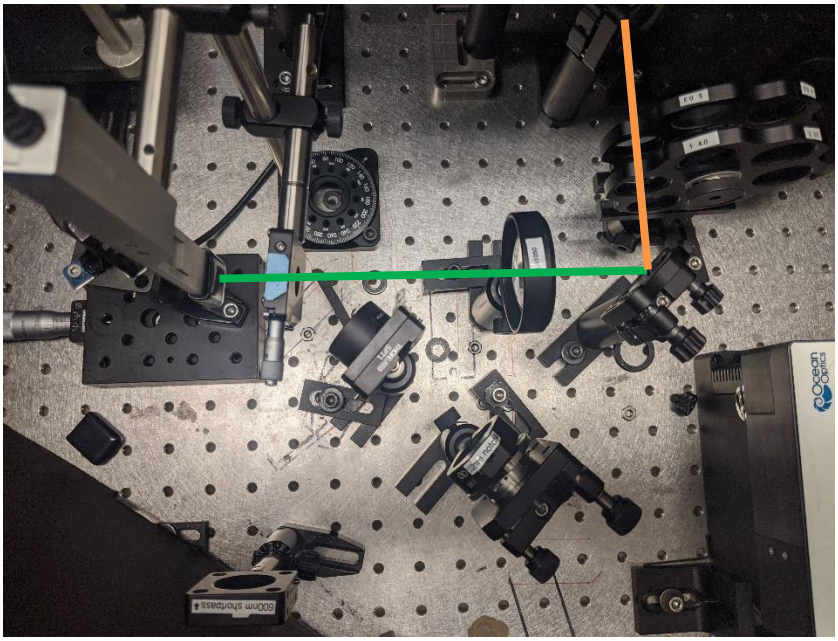

Figure 5.13 Photo of set up for beam diameter measurement with beam path of 532 nm laser labeled in green.

5.19 Transient absorption spectra of thin films

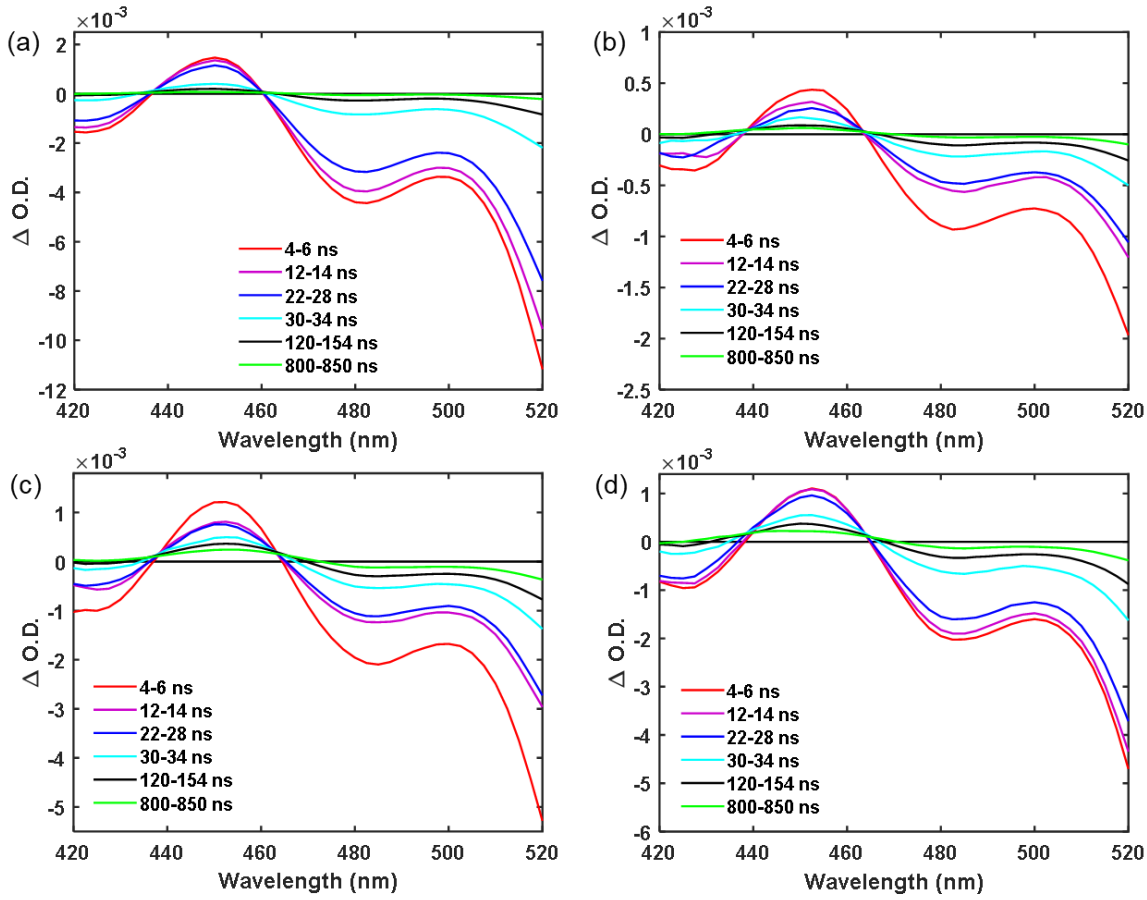

Figure 5.14 Transient absorption spectra for thin films of (a) CdSe/OA, (b) CdSe/9-ACA, (c) blended, and (d) layered morphology using 532 nm pulsed pump and xenon lamp probe light source on the envision transient absorption instrument.

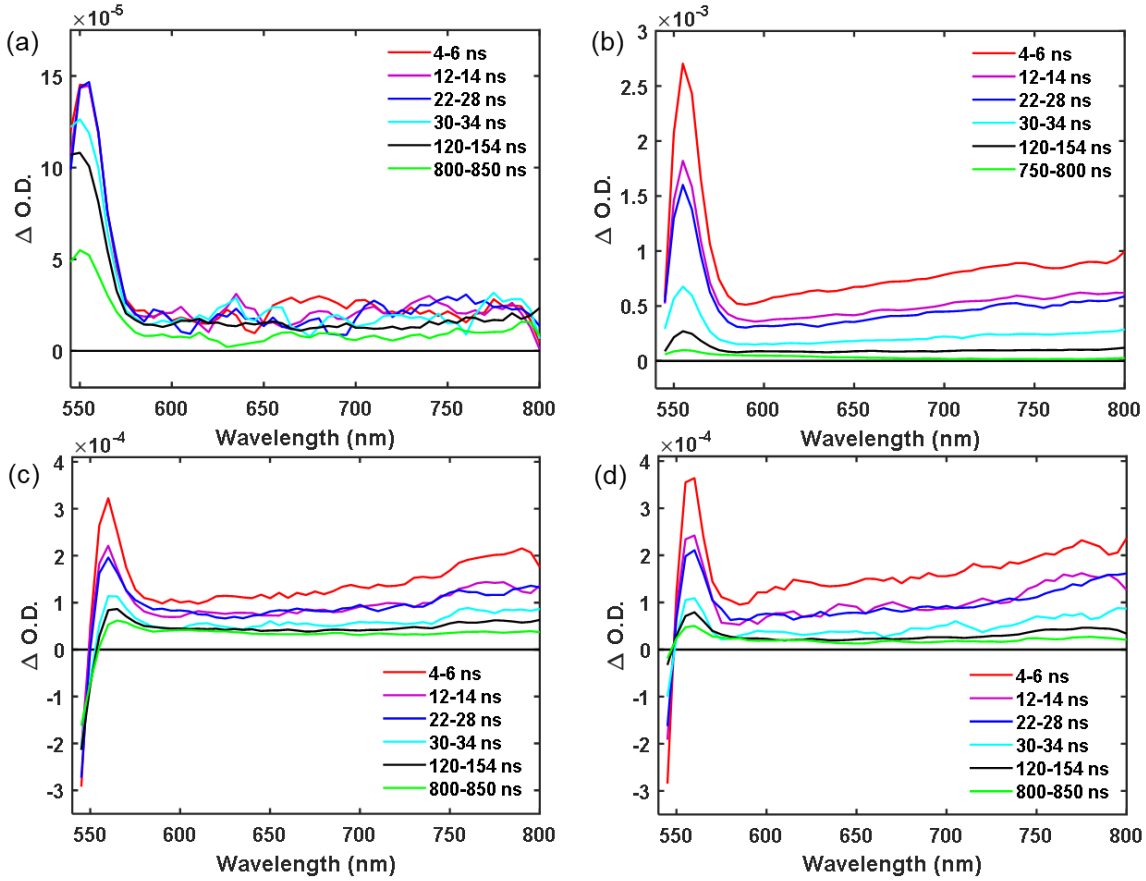

Figure 5.15 Transient absorption spectra for thin films of (a) CdSe/OA, (b) CdSe/9-ACA, (c) blended, and (d) layered morphology from 545nm to 800 nm.

5.20 PL spectra for blended film upconversion spots vs DPA in toluene

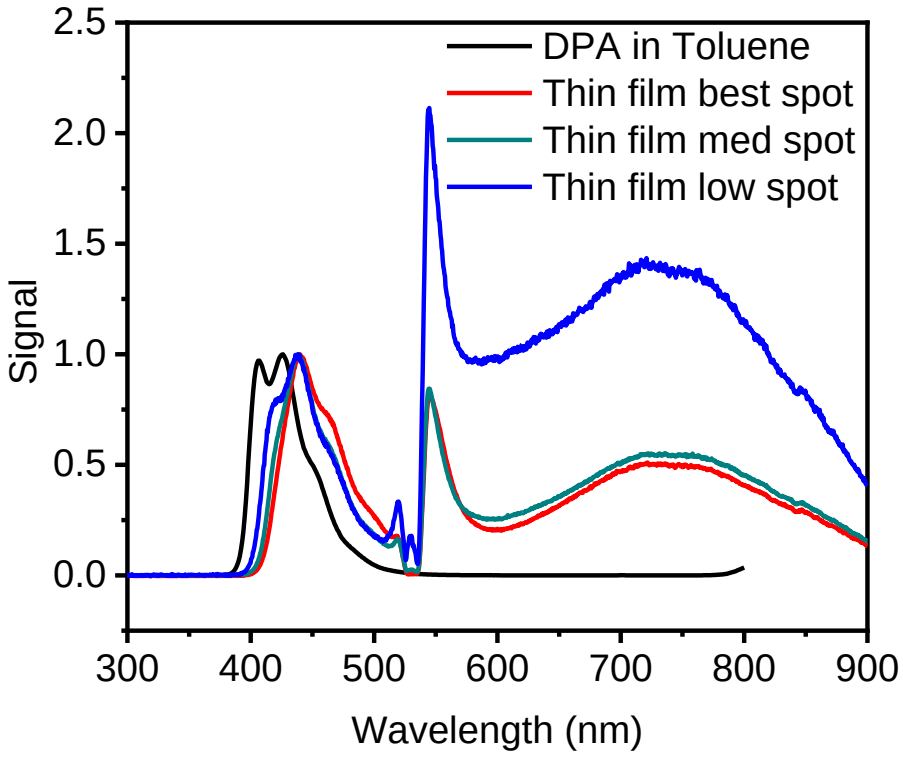

Figure 5.16 Normalized PL emission spectra for DPA in toluene (black trace) compared to the best, average, and low upconversion spots on the blended film morphology.

5.21 Transient absorption spectra after 0-20 ns early time subtraction

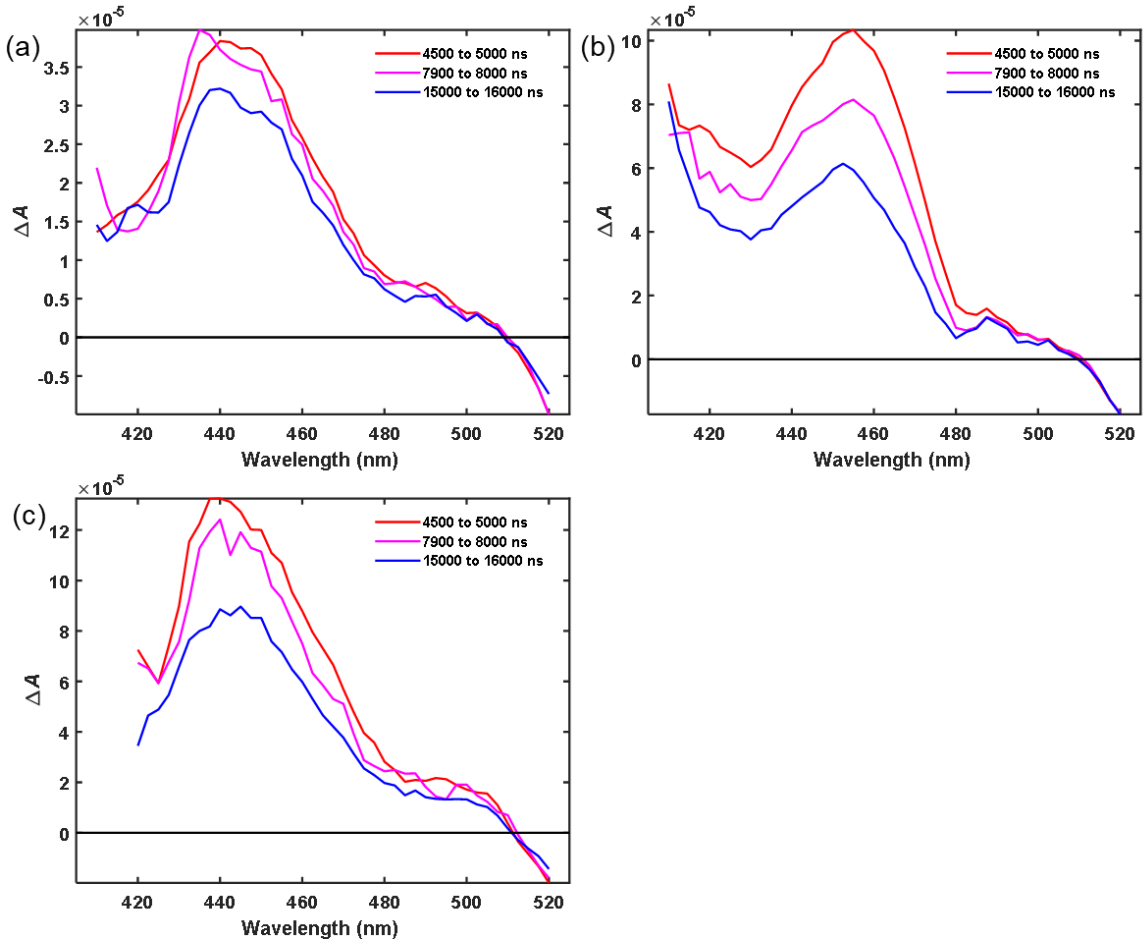

Figure 5.17 9-ACA triplet peak from the transient absorption data of (a) CdSe/9-ACA thin film, (b) blended thin film, and (c) layered thin film after subtraction of CdSe component from 0-20 ns.

5.22 Fits of transient absorption data and extraction of ϕ_{TET1}

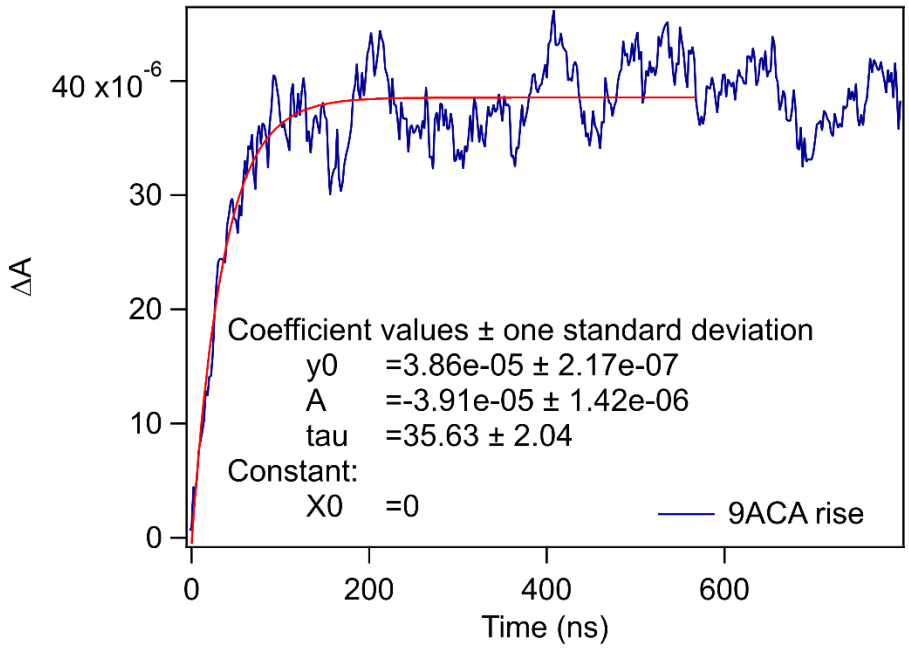

Figure 5.18 Fit of 9-ACA triplet rise on CdSe/9-ACA thin film with 0-20 ns CdSe component subtracted.

Φ_{TET1} is the efficiency of transfer from the CdSe NC absorber and the bound 9-ACA ligand. The lifetime of triplet transfer from CdSe to 9-ACA can be seen in Figure 5.18. The lifetime of CdSe/OA is taken from the amplitude weighted lifetime of the global fit of the CdSe/OA sample at 440 nm.

Table 5.7 Global fitting results from CdSe/OA transient absorption kinetics at 440 nm.

CdSe/OA			
A1	t1/ ns	A2	t2/ ns
0.000784	33.5	0.000118	958.5

Table 5.8 Amplitude weighted lifetime of CdSe/OA thin film at 440 nm and time constant of kTET1 in CdSe/9-ACA thin film with resulting Φ_{TET1} value.

Amplitude weighted lifetime (ns)	154.2
kTET1 (ns)	35.6
Φ_{TET1}	**0.813**

5.23 Global fitting equations and fitting parameters of transient absorption traces for thin film samples

NC with transmitter ligand (9-ACA) introducing additional triplet decay component: τ_2

$$I(t) = A_0 exp\left(-\frac{t-t_0}{\tau_1}\right) + A_1 exp\left(-\frac{t-t_0}{\tau_2}\right) \quad (5.12)$$

where t_0 is a time offset, A is the maximum absorption of the 9-ACA triplet, τ_1 corresponds to the intrinsic decay of the NC, and τ_2 is the net transfer of excited state energy between the nanocrystal and the 9-ACA ligand (τ_{TET1}). Using a global fit allows the intensity of absorption to vary with wavelength, while linking the lifetime components.

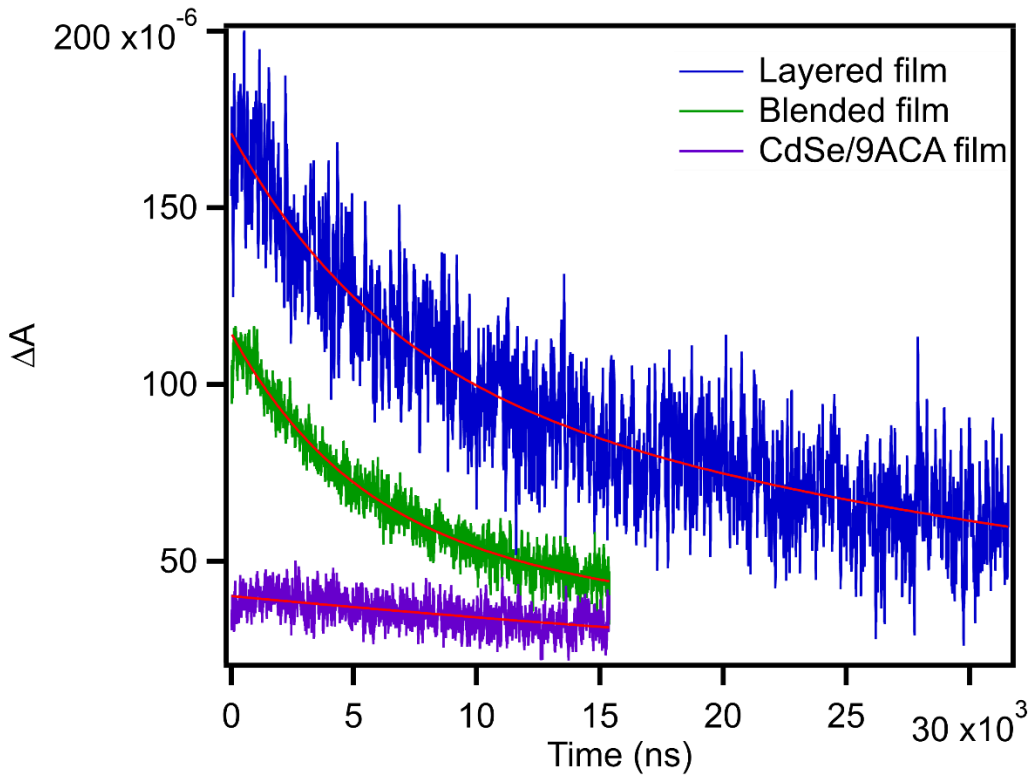

Figure 5.19 Global fitting of CdSe/9-ACA only film, layered film, and blended film at 440 nm showing the triplet lifetimes of each.

Table 5.9 Triplet lifetime data from global fitting results of thin films compared to triplet lifetime of CdSe/9-ACA measured in toluene solution.

Sample	***Triplet lifetime (μs)***
9-ACA in solution	260
9-ACA only film	61 ± 1.7
Blended film	5.1 ± 0.12
Layered film	6.5 ± 0.15

5.24 Photoluminescence mapping of blended and layered films

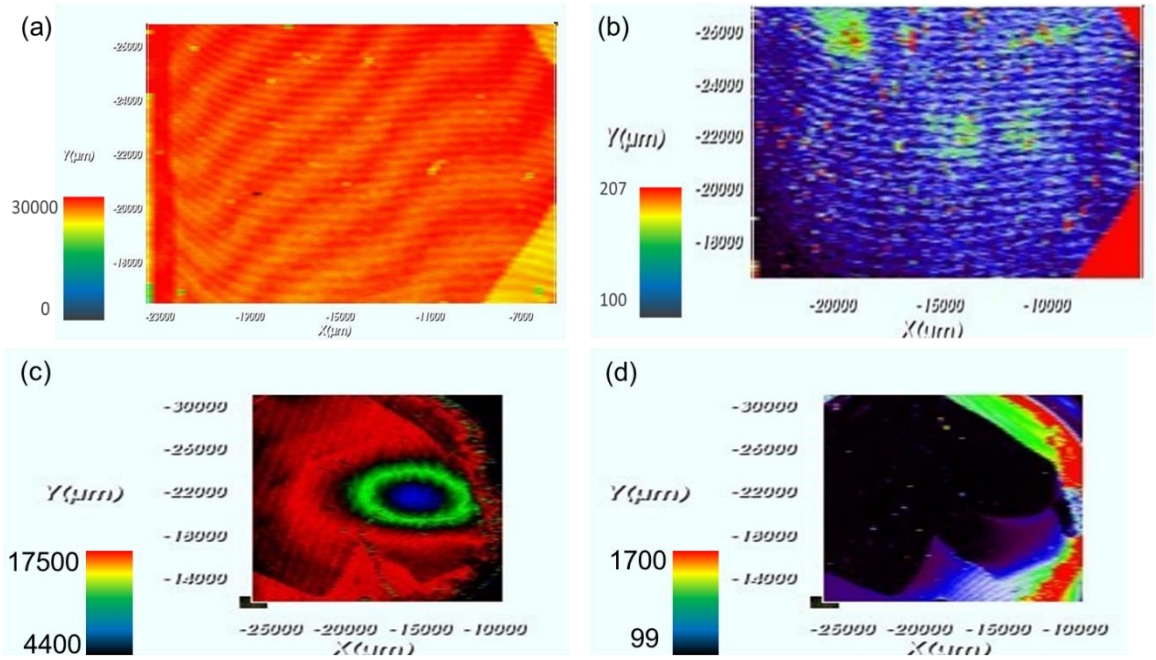

Figure 5.20 PL mapping from blended thin film with 405 nm excitation (a) mapping DPA distribution within the film, and 532 nm excitation (b) mapping CdSe distribution within the film. PL mapping from layered thin film with 405 nm excitation (c) showing DPA distribution and 532 nm (d) showing CdSe distribution within the film.

5.25 References

1. Otchy, T. M.; Wolff, S. B. E.; Rhee, J. Y.; Pehlevan, C.; Kawai, R.; Kempf, A.; Gobes, S. M. H.; Ölveczky, B. P., Acute off-target effects of neural circuit manipulations. *Nature* **2015,** *528* (7582), 358-363.

2. Khnayzer, R. S.; Blumhoff, J.; Harrington, J. A.; Haefele, A.; Deng, F.; Castellano, F. N., Upconversion of sub-band gap light in solar cell; powered photoelectrochemistry, WO3 nanostructured anode. *Chem. Commun. (Cambridge, U. K.)* **2012,** *48* (2), 209-211.

3. Mongin, C.; Garakyaraghi, S.; Razgoniaeva, N.; Zamkov, M.; Castellano, F. N., Direct observation of triplet energy transfer from semiconductor nanocrystals. *Science (Washington, DC, U. S.)* **2016,** *351* (6271), 369-372.

4. Huang, Z.; Li, X.; Mahboub, M.; Hanson, K. M.; Nichols, V. M.; Le, H.; Tang, M. L.; Bardeen, C. J., Hybrid Molecule-Nanocrystal Photon Upconversion Across the Visible and Near-Infrared. *Nano Lett.* **2015,** *15* (8), 5552-5557.

5. Wu, M.; Congreve, D. N.; Wilson, M. W. B.; Jean, J.; Geva, N.; Welborn, M.; Van Voorhis, T.; Bulovic, V.; Bawendi, M. G.; Baldo, M. A., Solid-state infrared-to-visible upconversion sensitized by colloidal nanocrystals. *Nat. Photonics* **2016,** *10* (1), 31-34.

6. Rigsby, E. M.; Miyashita, T.; Jaimes, P.; Fishman, D. A.; Tang, M. L., On the size-dependence of CdSe nanocrystals for photon upconversion with anthracene. *The Journal of Chemical Physics* **2020,** *153* (11), 114702.

7. Kim, W.; Lim, S. J.; Jung, S.; Shin, S. K., Binary Amine-Phosphine Passivation of Surface Traps on CdSe Nanocrystals. *J. Phys. Chem. C* **2010,** *114* (3), 1539-1546.

8. Galian, R. E.; Scaiano, J. C., Fluorescence quenching of CdSe quantum dots by tertiary amines and their surface binding effect. *Photochem. Photobiol. Sci.* **2009,** *8* (1), 70-74.

9. Rigsby, E. M.; Lee, K.; Sun, J.; Fishman, D. A.; Tang, M. L., Primary amines enhance triplet energy transfer from both the band edge and trap state from CdSe nanocrystals. *The Journal of Chemical Physics* **2019,** *151* (17), 174701.

10. Islangulov, R. R.; Lott, J.; Weder, C.; Castellano, F. N., Noncoherent Low-Power Upconversion in Solid Polymer Films. *Journal of the American Chemical Society* **2007,** *129* (42), 12652-12653.

11. Parker, C. A.; Hatchard, C. G., Triplet-singlet emission in fluid solutions. Phosphorescence of eosin. *Transactions of the Faraday Society* **1961,** *57* (0), 1894-1904.

12. Merkel, P. B.; Dinnocenzo, J. P., Low-power green-to-blue and blue-to-UV upconversion in rigid polymer films. *Journal of Luminescence* **2009,** *129* (3), 303-306.

13. Wohnhaas, C.; Turshatov, A.; Mailänder, V.; Lorenz, S.; Baluschev, S.; Miteva, T.; Landfester, K., Annihilation Upconversion in Cells by Embedding the Dye System in Polymeric Nanocapsules. *Macromolecular Bioscience* **2011,** *11* (6), 772-778.

14. Liu, Q.; Yang, T.; Feng, W.; Li, F., Blue-Emissive Upconversion Nanoparticles for Low-Power-Excited Bioimaging in Vivo. *Journal of the American Chemical Society* **2012,** *134* (11), 5390-5397.

15. Monguzzi, A.; Frigoli, M.; Larpent, C.; Tubino, R.; Meinardi, F., Low-Power-Photon Up-Conversion in Dual-Dye-Loaded Polymer Nanoparticles. *Advanced Functional Materials* **2012,** *22* (1), 139-143.

16. Hagstrom, A. L.; Lee, H.-L.; Lee, M.-S.; Choe, H.-S.; Jung, J.; Park, B.-G.; Han, W.-S.; Ko, J.-S.; Kim, J.-H.; Kim, J.-H., Flexible and Micropatternable Triplet–Triplet Annihilation Upconversion Thin Films for Photonic Device Integration and Anticounterfeiting Applications. *ACS Applied Materials & Interfaces* **2018,** *10* (10), 8985-8992.

17. Jankus, V.; Snedden, E. W.; Bright, D. W.; Whittle, V. L.; Williams, J. A. G.; Monkman, A., Energy Upconversion via Triplet Fusion in Super Yellow PPV Films Doped with Palladium Tetraphenyltetrabenzoporphyrin: a Comprehensive Investigation of Exciton Dynamics. *Advanced Functional Materials* **2013,** *23* (3), 384-393.

18. Kim, J.-H.; Deng, F.; Castellano, F. N.; Kim, J.-H., High Efficiency Low-Power Upconverting Soft Materials. *Chemistry of Materials* **2012,** *24* (12), 2250-2252.

19. Monguzzi, A.; Bianchi, F.; Bianchi, A.; Mauri, M.; Simonutti, R.; Ruffo, R.; Tubino, R.; Meinardi, F., High Efficiency Up-Converting Single Phase Elastomers for Photon Managing Applications. *Advanced Energy Materials* **2013,** *3* (5), 680-686.

20. Lissau, J. S.; Nauroozi, D.; Santoni, M.-P.; Edvinsson, T.; Ott, S.; Gardner, J. M.; Morandeira, A., What Limits Photon Upconversion on Mesoporous Thin Films Sensitized by Solution-Phase Absorbers? *The Journal of Physical Chemistry C* **2015,** *119* (9), 4550-4564.

21. Xia, P.; Raulerson, E. K.; Coleman, D.; Gerke, C. S.; Mangolini, L.; Tang, M. L.; Roberts, S. T., Achieving spin-triplet exciton transfer between silicon and molecular acceptors for photon upconversion. *Nature Chemistry* **2020,** *12* (2), 137-144.

22. Bullen, C.; Mulvaney, P., The Effects of Chemisorption on the Luminescence of CdSe Quantum Dots. *Langmuir* **2006,** *22* (7), 3007-3013.

23. Landes, C.; Burda, C.; Braun, M.; El-Sayed, M. A., Photoluminescence of CdSe Nanoparticles in the Presence of a Hole Acceptor: n-Butylamine. *J. Phys. Chem. B* **2001,** *105* (15), 2981-2986.

24. Kalyuzhny, G.; Murray, R. W., Ligand Effects on Optical Properties of CdSe Nanocrystals. *J. Phys. Chem. B* **2005,** *109* (15), 7012-7021.

25. Li, X.; Fast, A.; Huang, Z.; Fishman, D. A.; Tang, M. L., Complementary Lock-and-Key Ligand Binding of a Triplet Transmitter to a Nanocrystal Photosensitizer. *Angew. Chem., Int. Ed.* **2017,** *56* (20), 5598-5602.

26. Li, X.; Huang, Z.; Zavala, R.; Tang, M. L., Distance-Dependent Triplet Energy Transfer between CdSe Nanocrystals and Surface Bound Anthracene. *J. Phys. Chem. Lett.* **2016,** *7* (11), 1955-1959.

27. Xia, P.; Huang, Z.; Li, X.; Romero, J. J.; Vullev, V. I.; Pau, G. S. H.; Tang, M. L., On the efficacy of anthracene isomers for triplet transmission from CdSe nanocrystals. *Chem. Commun. (Cambridge, U. K.)* **2017,** *53* (7), 1241-1244.

28. Morris-Cohen, A. J.; Malicki, M.; Peterson, M. D.; Slavin, J. W. J.; Weiss, E. A., Chemical, Structural, and Quantitative Analysis of the Ligand Shells of Colloidal Quantum Dots. *Chem. Mater.* **2013,** *25* (8), 1155-1165.

29. Hens, Z.; Martins, J. C., A Solution NMR Toolbox for Characterizing the Surface Chemistry of Colloidal Nanocrystals. *Chem. Mater.* **2013,** *25* (8), 1211-1221.

30. Anderson, N. C.; Hendricks, M. P.; Choi, J. J.; Owen, J. S., Ligand Exchange and the Stoichiometry of Metal Chalcogenide Nanocrystals: Spectroscopic Observation of Facile Metal-Carboxylate Displacement and Binding. *J. Am. Chem. Soc.* **2013,** *135* (49), 18536-18548.

31. Gomes, R.; Hassinen, A.; Szczygiel, A.; Zhao, Q.; Vantomme, A.; Martins, J. C.; Hens, Z., Binding of Phosphonic Acids to CdSe Quantum Dots: A Solution NMR Study. *J. Phys. Chem. Lett.* **2011,** *2* (3), 145-152.

32. Mongin, C.; Moroz, P.; Zamkov, M.; Castellano, F. N., Thermally activated delayed photoluminescence from pyrenyl-functionalized CdSe quantum dots. *Nat. Chem.* **2018,** *10* (2), 225-230.

33. Nienhaus, L.; Wu, M.; Geva, N.; Shepherd, J. J.; Wilson, M. W. B.; Bulovic, V.; Van Voorhis, T.; Baldo, M. A.; Bawendi, M. G., Speed Limit for Triplet-Exciton Transfer in Solid-State PbS Nanocrystal-Sensitized Photon Upconversion. *ACS Nano* **2017,** *11* (8), 7848-7857.

34. Knowles, K. E.; McArthur, E. A.; Weiss, E. A., A Multi-Timescale Map of Radiative and Nonradiative Decay Pathways for Excitons in CdSe Quantum Dots. *ACS Nano* **2011,** *5* (3), 2026-2035.

35. Huang, J.; Huang, Z.; Jin, S.; Lian, T., Exciton Dissociation in CdSe Quantum Dots by Hole Transfer to Phenothiazine. *J. Phys. Chem. C* **2008,** *112* (49), 19734-19738.

36. Burda, C.; Link, S.; Mohamed, M.; El-Sayed, M., The Relaxation Pathways of CdSe Nanoparticles Monitored with Femtosecond Time-Resolution from the Visible to the IR: Assignment of the Transient Features by Carrier Quenching. *J. Phys. Chem. B* **2001,** *105* (49), 12286-12292.

37. Murov, S. L.; Carmichael, I.; Hug, G. L., *Handbook of photochemistry*. CRC Press: 1993.

38. Marcus, R. A., Theoretical relations among rate constants, barriers, and Broensted slopes of chemical reactions. *The Journal of Physical Chemistry* **1968,** *72* (3), 891-899.

39. Marcus, R. A.; Siders, P., Theory of highly exothermic electron transfer reactions. *The Journal of Physical Chemistry* **1982,** *86* (5), 622-630.

40. De Roo, J.; Huang, Z.; Schuster, N. J.; Hamachi, L. S.; Congreve, D. N.; Xu, Z.; Xia, P.; Fishman, D. A.; Lian, T.; Owen, J. S.; Tang, M. L., Anthracene Diphosphate Ligands for CdSe Quantum Dots; Molecular Design for Efficient Upconversion. *Chemistry of Materials* **2020,** *32* (4), 1461-1466.

41. Huang, Z.; Simpson, D. E.; Mahboub, M.; Li, X.; Tang, M. L., Ligand enhanced upconversion of near-infrared photons with nanocrystal light absorbers. *Chemical Science* **2016,** *7* (7), 4101-4104.

42. Huang, Z.; Xu, Z.; Mahboub, M.; Liang, Z.; Jaimes, P.; Xia, P.; Graham, K. R.; Tang, M. L.; Lian, T., Enhanced Near-Infrared-to-Visible Upconversion by Synthetic Control of PbS Nanocrystal Triplet Photosensitizers. *J. Am. Chem. Soc.* **2019,** *141* (25), 9769-9772.

43. Gray, V.; Küçüköz, B.; Edhborg, F.; Abrahamsson, M.; Moth-Poulsen, K.; Albinsson, B., Singlet and triplet energy transfer dynamics in self-assembled axial porphyrin–anthracene complexes: towards supra-molecular structures for photon upconversion. *Physical Chemistry Chemical Physics* **2018,** *20* (11), 7549-7558.

44. Andraos, J., A Streamlined Approach to Solving Simple and Complex Kinetic Systems Analytically. *Journal of Chemical Education* **1999,** *76* (11), 1578.

45. Mahboub, M.; Xia, P.; Van Baren, J.; Li, X.; Lui, C. H.; Tang, M. L., Midgap States in PbS Quantum Dots Induced by Cd and Zn Enhance Photon Upconversion. *ACS Energy Letters* **2018,** *3* (4), 767-772.

46. Han, Y.; He, S.; Luo, X.; Li, Y.; Chen, Z.; Kang, W.; Wang, X.; Wu, K., Triplet Sensitization by "Self-Trapped" Excitons of Nontoxic CuInS2 Nanocrystals for Efficient Photon Upconversion. *Journal of the American Chemical Society* **2019,** *141* (33), 13033-13037.

47. Mongin, C.; Moroz, P.; Zamkov, M.; Castellano, F. N., Thermally activated delayed photoluminescence from pyrenyl-functionalized CdSe quantum dots. *Nature Chemistry* **2018,** *10* (2), 225-230.

48. Nirmal, M.; Norris, D. J.; Kuno, M.; Bawendi, M. G.; Efros, A. L.; Rosen, M., Observation of the "dark exciton" in CdSe quantum dots. *Phys. Rev. Lett.* **1995,** *75* (20), 3728-31.

49. Crooker, S. A.; Barrick, T.; Hollingsworth, J. A.; Klimov, V. I., Multiple temperature regimes of radiative decay in CdSe nanocrystal quantum dots: Intrinsic limits to the dark-exciton lifetime. *Appl. Phys. Lett.* **2003,** *82* (17), 2793-2795.

50. Sercel, P. C.; Shabaev, A.; Efros, A. L., Photoluminescence Enhancement through Symmetry Breaking Induced by Defects in Nanocrystals. *Nano Lett.* **2017,** *17* (8), 4820-4830.

51. Korkusinski, M.; Voznyy, O.; Hawrylak, P., Fine structure and size dependence of exciton and biexciton optical spectra in CdSe nanocrystals. *Phys. Rev. B: Condens. Matter Mater. Phys.* **2010,** *82* (24), 245304/1-245304/16.

52. Califano, M.; Franceschetti, A.; Zunger, A., Lifetime and polarization of the radiative decay of excitons, biexcitons, and trions in CdSe nanocrystal quantum dots. *Phys. Rev. B: Condens. Matter Mater. Phys.* **2007,** *75* (11), 115401/1-115401/7.

53. Efros, A. L., Fine structure and polarization properties of the band edge excitons in semiconductor nanorystals. In *Semiconductor and Metal Nanocrystals: Synthesis and Elctronic and Optical Properties*, Klimov, V. I., Ed. Marcel Dekker: New York, 2003; p 103.

54. Efros, A. L.; Rosen, M.; Kuno, M.; Nirmal, M.; Norris, D. J.; Bawendi, M., Band-edge exciton in quantum dots of semiconductors with a degenerate valence band: dark and bright exciton states. *Phys. Rev. B: Condens. Matter* **1996,** *54* (7), 4843-4856.

55. Xu, Z.; Huang, Z.; Li, C.; Huang, T.; Evangelista, F. A.; Tang, M. L.; Lian, T., Tuning the Quantum Dot (QD)/Mediator Interface for Optimal Efficiency of QD-Sensitized Near-Infrared-to-Visible Photon Upconversion Systems. *ACS Applied Materials & Interfaces* **2020**.

56. Khnayzer, R. S.; Blumhoff, J.; Harrington, J. A.; Haefele, A.; Deng, F.; Castellano, F. N., Upconversion-powered photoelectrochemistry. *Chem. Commun.* **2012,** *48* (2), 209-211.

57. Mongin, C.; Garakyaraghi, S.; Razgoniaeva, N.; Zamkov, M.; Castellano, F. N., Direct observation of triplet energy transfer from semiconductor nanocrystals. *Science* **2016,** *351* (6271), 369-372.

58. Ravetz, B. D.; Pun, A. B.; Churchill, E. M.; Congreve, D. N.; Rovis, T.; Campos, L. M., Photoredox catalysis using infrared light via triplet fusion upconversion. *Nature* **2019,** *565* (7739), 343-346.

59. Mattos, D. F. B. d.; Dreos, A.; Johnstone, M. D.; Runemark, A.; Sauvée, C.; Gray, V.; Moth-Poulsen, K.; Sundén, H.; Abrahamsson, M., Covalent incorporation of diphenylanthracene in oxotriphenylhexanoate organogels as a quasi-solid photon upconversion matrix. *The Journal of Chemical Physics* **2020,** *153* (21), 214705.

60. Li, X.; Fast, A.; Huang, Z. Y.; Fishman, D. A.; Tang, M. L., Complementary Lock-and-Key Ligand Binding of a Triplet Transmitter to a Nanocrystal Photosensitizer. *Angew. Chem.-Int. Edit.* **2017,** *56* (20), 5598-5602.

61. Li, X.; Huang, Z.; Zavala, R.; Tang, M. L., Distance-Dependent Triplet Energy Transfer between CdSe Nanocrystals and Surface Bound Anthracene. *Journal of Physical Chemistry Letters* **2016,** *7* (11), 1955–1959.

62. Di, D.; Yang, L.; Richter, J. M.; Meraldi, L.; Altamimi, R. M.; Alyamani, A. Y.; Credgington, D.; Musselman, K. P.; MacManus-Driscoll, J. L.; Friend, R. H., Efficient Triplet Exciton Fusion in Molecularly Doped Polymer Light-Emitting Diodes. *Advanced Materials* **2017,** *29* (13), 1605987.

63. Lin, T.-A.; Perkinson, C. F.; Baldo, M. A., Strategies for High-Performance Solid-State Triplet–Triplet-Annihilation-Based Photon Upconversion. *Advanced Materials* **2020,** *32* (26), 1908175.

64. Cheng, Y. Y.; Khoury, T.; Clady, R. G. C. R.; Tayebjee, M. J. Y.; Ekins-Daukes, N. J.; Crossley, M. J.; Schmidt, T. W., On the efficiency limit of triplet–triplet annihilation for photochemical upconversion. *Physical Chemistry Chemical Physics* **2010,** *12* (1), 66-71.

65. Ogawa, T.; Hosoyamada, M.; Yurash, B.; Nguyen, T.-Q.; Yanai, N.; Kimizuka, N., Donor–Acceptor–Collector Ternary Crystalline Films for Efficient Solid-State Photon Upconversion. *Journal of the American Chemical Society* **2018,** *140* (28), 8788-8796.

66. Huang, Z.; Xu, Z.; Huang, T.; Gray, V.; Moth-Poulsen, K.; Lian, T.; Tang, M. L., Evolution from Tunneling to Hopping Mediated Triplet Energy Transfer from Quantum Dots to Molecules. *Journal of the American Chemical Society* **2020,** *142* (41), 17581-17588.

67. Zhang, J.; Gao, J.; Church, C. P.; Miller, E. M.; Luther, J. M.; Klimov, V. I.; Beard, M. C., PbSe Quantum Dot Solar Cells with More than 6% Efficiency Fabricated in Ambient Atmosphere. *Nano Letters* **2014,** *14* (10), 6010-6015.

68. Leyre, S.; Coutino-Gonzalez, E.; Joos, J. J.; Ryckaert, J.; Meuret, Y.; Poelman, D.; Smet, P. F.; Durinck, G.; Hofkens, J.; Deconinck, G.; Hanselaer, P., Absolute determination of photoluminescence quantum efficiency using an integrating sphere setup. *Review of Scientific Instruments* **2014,** *85* (12), 123115.